Computers and Structures 164 (2016) 108–126

Contents lists available at ScienceDirect

Computers and Structures

journal homepage: www.elsevier.com/locate/compstruc

# Free vibration analysis for plates with arbitrary boundary conditions using a novel spectral-dynamic stiffness method

X. Liu *, J.R. Banerjee

*School of Mathematics, Computer Science & Engineering, City University London, London EC1V 0HB, UK*

ARTICLE INFO

*Article history:*
Received 21 February 2015
Accepted 7 November 2015

*Keywords:*
Spectral-dynamic stiffness method
Free vibration of plates
Arbitrary boundary conditions
Wittrick–Williams algorithm
Analytical methods

ABSTRACT

An exact method for free vibration analysis of plates with arbitrary boundary conditions is presented. This is achieved by integrating the spectral method into the classical dynamic stiffness method. The formulation satisfies the governing differential equation exactly and any arbitrary boundary conditions are satisfied in a series sense. The Wittrick–Williams algorithm is enhanced with several elegant techniques to obtain solutions. The exactness and computational efficiency of the method are demonstrated by comparing results obtained from other methods. Finally, mathematical and physical insights are gained and significant conclusions are drawn for various analytical methods for free vibration analysis of plates.



## 1. Introduction

The free vibration of rectangular plates is a historical problem [1] for over two centuries which has given birth to many fundamental methods like the Rayleigh [2] and the Ritz [3] methods. This problem has also been a standard benchmark for many other analytical and numerical methods. However, the exact solutions for the problem are available only for Navier or Levy-type plates where at least one pair of opposite edges must be simply [4] and/or guided [5] supported. For more general boundary conditions, one needs to resort to approximate methods leading to approximate results.

The purpose of this paper is to develop a novel spectral-dynamic stiffness method (S-DSM) for free vibration analysis of plates with arbitrary boundary conditions to arrive at the exact solution. The superiority of the S-DSM also enables a comparative discussion on a wide range of analytical methods for free vibration analysis of plates.

Before embarking on the proposed method, some of the widely used typical analytical methods are reviewed first. These can be classified into two categories: weak-form based methods and strong-form based methods. The weak-form based methods have been frequently used, including for example, Rayleigh [2], Ritz [3] and Kantorovich [6] methods. In these methods, the governing differential equation (GDE) and sometimes the boundary conditions (BC) are satisfied in a variational sense. On the other hand, strong-form based methods obtain solutions satisfying both the GDE and BC in a strong manner, e.g., superposition method [7–9], generalised Koialovich's limitant theory based on superposition method [10], Fourier series based analytical method [11,12] and dynamic stiffness method [13]. Clearly, the proposed S-DSM belongs to the latter category.

The Rayleigh [2] and the Ritz [3] methods have been extensively used in the free vibration analysis of plates due to their flexibility and conceptual simplicity. These types of methods assume a superposition (linear combination) of admissible (or named as basis/trial/shape) functions. The geometric boundary conditions are satisfied by the chosen admissible functions or by using the penalty method. Then the unknown coefficients of the admissible functions are to be determined by minimising the energy functional of the system. The admissible functions including for example, beam characteristic functions [14,15], boundary characteristic orthogonal polynomials [16–18], orthogonal plate functions (sometimes called *pb*-2 polynomials) [19–22] and many others. However, the above methods may become numerically unstable when the admissible functions are evaluated at higher orders [23] creating ill-conditioned mass and stiffness matrices. To cope with this problem, Beslin and Nicolas [23] proposed a set of hierarchical trigonometric functions which was applied by Dozio [24] for free vibration analysis of rectangular plates with various boundary condition. Also, the combination of trigonometric function and lower-order polynomials [25–29] have been used to avoid the aforementioned numerical problem. However, it appears that the convergence rate of these methods is still comparatively slow and the analysis is only limited to low to medium frequency ranges. The Kantorovich method [6] together

* Corresponding author.
*E-mail address:* xiangliu06@gmail.com (X. Liu).

http://dx.doi.org/10.1016/j.compstruc.2015.11.005
0045-7949/

with its derivatives [30–33] belong to another type of weak-form based methods. This type of methods approximate the deformation as the product of an unknown function in one spatial variable and an assumed function of both variables. In this way the original partial differential equation (PDE) is reduced into an ordinary differential equation (ODE) in the unknown function. The Kantorovich method [6] was later extended by Kerr [30] by considering the original Kantorovich method to be just a single step in an iterative process. The extended method was applied by Jones and Milne [31] and Sakata et al. [32] for free vibration analysis of rectangular plates. Then the extended version was further modified [33] by replacing the iterative process with two simultaneous ODEs which can be solved analytically. The authors of Ref. [33] emphasised that the method is simpler than their contemporary methods such as the Ritz method. However, the results of all versions of Kantorovich method always have discrepancy with accurate solutions. This is due to the nature of the method which will be explained later in Sections 5 and 6.

It should be recognised that even though different strong-form based methods have different procedures, they are all somehow based on superposition method which was pioneered by Lamé [34] and then used by Iguchi [35] to discuss free vibration of a completely free plate. Gorman [7,8] developed an accurate and systematic superposition method for plates to perform modal analysis of plates with different boundary conditions. The method essentially decomposes classical boundary conditions into a set of cases whose analytical solutions are available in series form. Kshirsagar and Bhaskar [9] extended the superposition method by using the so-called untruncated infinite series (although the method did use truncated moment series for non-Levy cases) to obtain highly accurate results. However, their formulation seems to be inapplicable to the cases with two adjacent free edges. Meleshko and Papkov [10] and Papkov and Banerjee [36] enhanced the superposition method by taking advantage of the regularity of the ensuing infinite algebraic system. By using the generalised Koialovich's limitant theory [37], the upper and lower bounds of the eigenvalues were predicted in [10,36]. Nevertheless, the formulations given in Refs. [10,36] are quite complex even for the most specific cases in which all of the plate edges are free [10] or clamped [36]. Sakata and Hosokawa [38] used an iteration method with superposition of double trigonometric series satisfying part of the BC and then the GDE, while the rest of the BC led to a linear algebraic equation to obtain very accurate results. The method appears to have been reported only for fully clamped plates but with very slow convergence rate. Xing and his coauthors [39–41] proposed a novel separation of variables method for free vibration analysis of rectangular plates with classical boundary conditions. Unfortunately it was later pointed out by Bahrami et al. [42] that this method does not give exact solutions for non-Levy type plates. Lim et al. used a symplectic elasticity method [43] for exact free vibration of Levy-type rectangular plates [44]. However, if this method is applied to non-Levy-type plates [45], inaccuracy may occur due to similar reason that arises from other methods [39–41]. This will be explained later in Section 6. Evidently, in the above mentioned superposition or related methods, different BC require different formulations. To solve this problem, Li and his coauthors [11,12] proposed a Fourier-series based analytical method for plates with general boundary supports. In this method, by using a fictitious Fourier cosine series to first satisfy the elastic BC then the GDE, the final eigenvalue system is expressed by separate stiffness and mass matrices. This method uses a complete set of series to deal with plates having elastic boundary conditions. However, the basic concept of this method lies in using the elastic BC as penalty parameters to model different BC, which may lead to ill-conditioning stiffness or mass matrices and becomes an obstacle for this method to obtain highly accurate results, particularly in the higher frequency range.

The dynamic stiffness method (DSM) [13], or sometimes called the spectral element method (SEM) [46] is another type of strong-form based elegant method which provides exact solutions for Levy-type plates and plate assemblies. The DSM is highly computationally efficient and accurate because the dynamic stiffness formulation is based on exact shape function, which has much lower degrees of freedom than that of the FEM. In addition, the application of the Wittrick–Williams algorithm [47] enables one to compute any required natural frequencies at any desired accuracy, and the algorithm ensures that no natural frequency will be missed. In the past decades, numerous exact dynamic stiffness theories have been developed for a wide range of one-dimensional (1D) elements such as rods and beams. For two dimensional elements like plates, the DSM has been developed by using different plate theories [48–53]. Nevertheless, all of these investigations were restricted to cases where at least a pair of opposite edges of the plate are simply supported to enable a Levy solution. This imposed severe limitation to prevent the DSM application for the general case.

The main difficulty encountered in the DS formulation for a 2D plate with arbitrary boundary conditions lies in obtaining the dynamic shape functions. This set of shape functions should capture all possible deformation governed by the GDE, and also it must be capable of providing accurate representation for arbitrarily prescribed boundary conditions on the plate edges. These arbitrary continuous functions within a 2D domain cannot be easily expressed in a simple analytical form because of their arbitrariness. This difficulty is addressed in this paper by using the spectral method (the letter S is justifiably used in the name S-DSM). The general idea of spectral method is to represent an arbitrary function by an infinite series of functions (modified Fourier). In other words, the modified Fourier series is used to facilitate the choice of any desired freedom to cope with the arbitrariness of plate motion subjected to arbitrary boundary conditions. Mathematically, it provides a robust formulation to reduce the differential order of the governing differential equation (GDE) by introducing the corresponding parameters like the frequency and the wavenumbers. Physically, the concept of 'spectral' has built a bridge between the wave propagation and structural vibration, which helps understand the physics behind the vibration problem. Throughout this paper the term 'spectral' is applied in both time and spatial domains. The spectral Fourier Transform (FT) of the time coordinate is referred as 'frequency' whilst the spectral modified FT of the spatial coordinates is defined as 'wavenumber'. It should be emphasised that the spectral in the current S-DSM is somehow different from the spectral element method (SEM) used by Patera [54], Ostachowica et al. [55] and Lee [46]. In [54,55], 'spectral' of SEM is used only for spatial coordinates and the 'spectral' in the latter [46] is only applied for time coordinate.

The current paper is organised as follows. In Section 2, the exact general solution is derived using the spectral method, which is then partitioned into four components with different symmetric or antisymmetric properties. In Section 3.1, the corresponding spectral-dynamic stiffness (S-DS) matrices for these four component cases are derived through a mixed-variable formulation procedure. Subsequently in Section 3.2, these S-DS component matrices are assembled to form the S-DS matrix for the entire plate. To this end, any prescribed boundary conditions can be transformed to modified Fourier series whose coefficients are related by the S-DS matrix. As the solution technique, the Wittrick–Williams algorithm is enhanced by a couple of novel techniques to resolve the mode count problem of a fully clamped plate, see Section 4. In Section 5, exact natural frequencies are computed using the current S-DSM for plates with different boundary conditions which are validated and compared with existing methods. Numerical simulations reveal that the current S-DSM is remarkably efficient and yet it gives exact results.

Comprehensive comparisons using a wide range of different methods made it possible to draw some general conclusions on various analytical (and exact) methods for free vibration analysis of plates, which are included in Section 6. The presentation is completed with conclusions in Section 7.

## 2. Governing differential equation and general solution

A rectangular Kirchhoff plate of dimension $2a \times 2b$ undergoing transverse free vibration is shown in Fig. 1. Based on the customary harmonic oscillation assumption, the transverse displacement $W(x,y)$ is described by the frequency-dependent GDE as [56]:

$$\frac{\partial^4 W}{\partial x^4} + 2\frac{\partial^4 W}{\partial x^2 \partial y^2} + \frac{\partial^4 W}{\partial y^4} + \chi\left(\frac{\partial^2 W}{\partial x^2} + \frac{\partial^2 W}{\partial y^2}\right) - kW = 0, \tag{1}$$

where

$$\kappa = \frac{\rho h \omega^2}{D}, \quad \chi = \frac{\rho h^3 \omega^2}{12D}, \quad D = \frac{Eh^3}{12(1-\nu^2)}. \tag{2}$$

In Eq. (1) above, $\omega$ is the circular frequency, hence both $\kappa$ and $\chi$ are frequency dependent parameters: $\kappa$ is inertia related while $\chi$ is rotatory inertia related. $D$ is the bending rigidity of the plate, $E$ is the Young's modulus of material, $\nu$ is the Poisson ratio, $h$ and $\rho$ are respectively the thickness and mass density of the plate. The natural boundary conditions on the four plate edges can be expressed through Hamilton's principle [56] as

$$\delta W : V_x \quad \text{and} \quad \delta\phi_x : M_x \quad \text{along} \quad x = \pm a, \tag{3a}$$

$$\delta W : V_y \quad \text{and} \quad \delta\phi_y : M_y \quad \text{along} \quad y = \pm b. \tag{3b}$$

Here, $\phi_x$ and $\phi_y$ are the rotation of the transverse normals on the boundary about $y$ and $x$ axes respectively, $M_x, M_y$ are bending moments and $V_x, V_y$ are effective shear forces on the corresponding boundaries. Following the sign conventions illustrated in Fig. 1, one can write

$$\phi_x = -\frac{\partial W}{\partial x}; \quad \phi_y = -\frac{\partial W}{\partial y}; \tag{4a}$$

$$M_x = -D\left(\frac{\partial^2 W}{\partial x^2} + \nu\frac{\partial^2 W}{\partial y^2}\right); \quad M_y = -D\left(\frac{\partial^2 W}{\partial y^2} + \nu\frac{\partial^3 W}{\partial x^2}\right); \tag{4b}$$

$$V_x = -D\left(\frac{\partial^3 W}{\partial x^3} + \Gamma^*\frac{\partial^3 W}{\partial x \partial y^2} + \chi\frac{\partial W}{\partial x}\right);$$

$$V_y = -D\left(\frac{\partial^3 W}{\partial y^3} + \Gamma^*\frac{\partial^3 W}{\partial y \partial x^2} + \chi\frac{\partial W}{\partial y}\right); \tag{4c}$$

where $\Gamma^* = 2 - \nu$.

It should be mentioned that the general solution of a plate equation with arbitrary boundary conditions is much more difficult to obtain than that for a beam or a Levy-type plate. This will be evident when looking at the characteristic equation. The general solution of Eq. (1) can be sought by using the method of separation of variables

$$W(x,y) = X(x)Y(y) = Ce^{qx+py}, \tag{5}$$

where $C$ is an arbitrary constant, $q$ and $p$ are wave parameters in the $x$ and $y$ directions respectively. Substituting Eq. (5) into Eq. (1) leads to the following characteristic equation

$$q^4 + 2q^2p^2 + p^4 + \chi(q^2 + p^2) - \kappa = 0, \tag{6}$$

which gives the dispersion (spectrum) relation by relating the frequency $\omega$ (in the form of $\kappa$ and $\chi$) with the wave parameters $q$ and $p$. Here we mention in passing that the general solution of a plate has an interesting parallel with the DSM formulation for one-dimensional (1D) elements such as a beam. For a beam, there is only one wave parameter in the characteristic equation. Therefore, the roots of the characteristic equation for beam problems will have only one wave parameter which can be expressed analytically in terms of the frequency. However, for a two dimensional (2D) element like plate, there will be two wave parameters in the characteristic equation as in Eq. (6). Thus, any combination of the wave parameters $q, p$ and frequency $\omega$ (in terms of $\kappa$ and $\chi$) satisfying Eq. (6) represents a solution to the governing Eq. (1). So there are infinite number of possibilities of such combinations. This is a formidable problem. (For Levy-type plate theories [48,49,53], this is simple because one of the wave parameters, which corresponds to the direction where opposite edges are simply supported, can be assumed to be fixed. The roots of the other wave parameter can be expressed in an analytical form just like that of a 1D element.)

As mentioned in the introduction, the difficulty for the plate problems for the general case can be resolved by incorporating the idea of spectral method in terms of modified Fourier series. Essentially, the general solution is composed of two infinite series, in each of which the solution in one directions (either $X(x)$ or $Y(y)$) in Eq. (5) can be expressed by the modified Fourier basis function of Eq. (A.1), see Appendix A

$$X(x) = \sum_{\substack{m\in\mathbb{N} \\ k\in\{0,1\}}} \widetilde{C}_{km}\mathcal{T}_k(\alpha_{km}x), \quad Y(y) = \sum_{\substack{n\in\mathbb{N} \\ j\in\{0,1\}}} \widetilde{C}_{jn}\mathcal{T}_j(\beta_{jn}y), \tag{7}$$

where $\widetilde{C}_{km}$ and $\widetilde{C}_{jn}$ are unknowns, $\mathbb{N} = \{0,1,2,3,\ldots\}$ is the non-negative integer set, and $\mathcal{T}_k$ and $\mathcal{T}_j$ are trigonometric functions forming a complete orthogonal set defined in Eq. (A.1) with the wavenumbers $\alpha_{km}$ and $\beta_{jn}$ taking the carefully chosen forms as shown below

$$\alpha_{km} = \begin{cases} \frac{m\pi}{a} & k = 0 \\ \left(m + \frac{1}{2}\right)\frac{\pi}{a} & k = 1 \end{cases}, \quad \beta_{jn} = \begin{cases} \frac{n\pi}{b} & j = 0 \\ \left(n + \frac{1}{2}\right)\frac{\pi}{b} & j = 1 \end{cases}. \tag{8}$$

The above formulation in Eqs. (7) and (8) is the first key step taken in the current S-DSM. Any arbitrary 1D function $X(x)$ or $Y(y)$ with

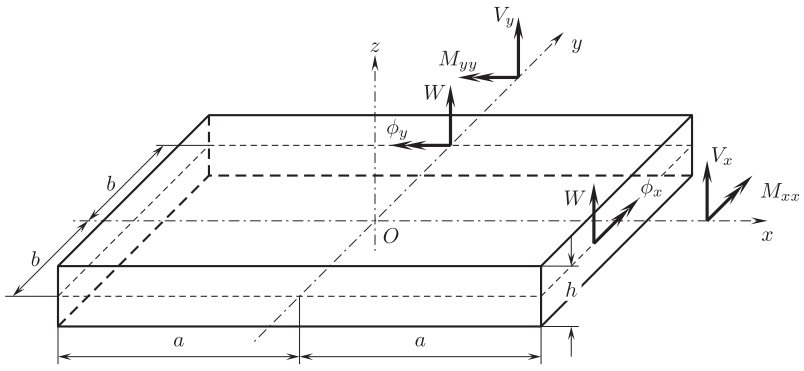


**Fig. 1.** Coordinate system and notations for displacements and forces for a thin plate.

arbitrary boundary conditions at its end ($x=\pm a$ or $y=\pm b$) is represented by the above complete orthogonal modified Fourier series with an infinite set of discrete wavenumbers. The series can be further partitioned into two parts, namely, symmetric and antisymmetric components. Then for each wavenumber in one direction, one can solve the solution analytically in the other direction. To this end, summing up the above two infinite series generated from Eq. (7) and based on Euler's formula, the general solution of the GDE of Eq. (1) can be expressed as

$$\begin{aligned} W(x,y) = &\sum_{\substack{m\in\mathbb{N}\\ k\in\{0,1\}}} \mathcal{T}_k(\alpha_{km}x)\Big[\widetilde{A}_{km1}\cosh(p_{1km}y)+\widetilde{A}_{km2}\cosh(p_{2km}y)\\ &+\widetilde{A}_{km3}\sinh(p_{1km}y)+\widetilde{A}_{km4}\sinh(p_{2km}y)\Big]\\ &+\sum_{\substack{n\in\mathbb{N}\\ j=\{0,1\}}} \mathcal{T}_j(\beta_{jn}y)\Big[\widetilde{B}_{jn1}\cosh(q_{1jn}x)+\widetilde{B}_{jn2}\cosh(q_{2jn}x)\\ &+\widetilde{B}_{jn3}\sinh(q_{1jn}x)+\widetilde{B}_{jn4}\sinh(q_{2jn}x)\Big], \end{aligned} \tag{9}$$

in which $\widetilde{A}_{km1}\sim\widetilde{A}_{km4}$ and $\widetilde{B}_{jn1}\sim\widetilde{B}_{jn4}$ are unknowns. The above wave parameters $p_{1km}, p_{2km}$ and $q_{1jn}, p_{2km}$ are obtained by substituting $q_{km}=i\alpha_{km}$ and $p_{jn}=i\beta_{jn}$ into the characteristic Eq. (6) to give

$$\text{either}\quad p_{1km}=\sqrt{\alpha_{km}^2-\frac{\chi}{2}-\sqrt{\frac{\chi^2}{4}+\kappa}},\quad p_{2km}=\sqrt{\alpha_{km}^2-\frac{\chi}{2}+\sqrt{\frac{\chi^2}{4}+\kappa}}, \tag{10a}$$

$$\text{or}\quad q_{1jn}=\sqrt{\beta_{jn}^2-\frac{\chi}{2}-\sqrt{\frac{\chi^4}{2}+\kappa}},\quad q_{2jn}=\sqrt{\beta_{jn}^2-\frac{\chi}{2}+\sqrt{\frac{\chi^4}{2}+\kappa}}. \tag{10b}$$

It should be noted that the general solution of Eq. (9) forms a complete set satisfying the GDE of Eq. (1). This is one of the most important techniques used to make the current method converge to the exact results with a very fast convergence rate with respect to the number of terms used in the series. The discussion of this particular aspect will be made in detail in Section 6 when comparison will be made with the series used in a wide range of other analytical methods. By considering the symmetry/antisymmetry of the hyperbolic and trigonometric functions, the general solution of Eq. (9) can be partitioned into a sum of four solution components $W^{kj}(x,y)$ as

$$W(x,y)=\sum_{k,j\in\{0,1\}} W^{kj}(x,y)=W^{00}+W^{01}+W^{10}+W^{11}, \tag{11}$$

where all of the four components of solution take the following concise form:

$$\begin{aligned} W^{kj}=&\sum_{m\in\mathbb{N}}\big[A_{1km}\mathcal{H}_j(p_{1km}y)+A_{2km}\mathcal{H}_j(p_{2km}y)\big]\mathcal{T}_k(\alpha_{km}x)\\ &+\sum_{n\in\mathbb{N}}\big[B_{1jn}\mathcal{H}_k(q_{1jn}x)+B_{2jn}\mathcal{H}_k(q_{2jn}x)\big]\mathcal{T}_j(\beta_{jn}y). \end{aligned} \tag{12}$$

In Eqs. (11) and (12), indices $k$ and $j$ denote respectively the symmetry relating to $x$ and $y$ axes. For example, $k$ taking '0' or '1' denotes an even or odd function in $x$ respectively. In Eq. (12), $A_{1km}, A_{2km}, B_{1jn}$ and $B_{2jn}$ are unknown coefficients to be eliminated, $\mathcal{T}$ is trigonometric functions defined in Eq. (A.1) of Appendix A and $\mathcal{H}$ stands for hyperbolic functions defined as follows:

$$\mathcal{H}_l(\Gamma\xi)=\begin{cases}\cosh(\Gamma\xi), & l=0\\ \sinh(\Gamma\xi), & l=1\end{cases} \tag{13}$$

with

$$\text{either}\quad \xi=x,\ l=k,\ \Gamma=p_{1km}\text{ or }p_{2km} \tag{14a}$$

$$\text{or}\quad \xi=y,\ l=j,\ \Gamma=q_{1jn}\text{ or }q_{2jn}. \tag{14b}$$

Before proceeding with further development, some of the differential properties of the hyperbolic $\mathcal{H}$ and trigonometric $\mathcal{T}$ functions are to be made use of. By introducing the notation

$$\mathcal{H}_l^*(\Gamma\xi)=\frac{\mathrm{d}\mathcal{H}_l(\Gamma\xi)}{\Gamma\mathrm{d}\xi}, \tag{15}$$

one has

$$\frac{\mathrm{d}^i\mathcal{H}_l(\Gamma\xi)}{\mathrm{d}\xi^i}=\begin{cases}\Gamma^i\mathcal{H}_l(\Gamma\xi) & i\text{ is even}\\ \Gamma^{i-1}\mathcal{H}_l^*(\Gamma\xi) & i\text{ is odd}\end{cases} \tag{16}$$

and

$$\frac{\mathrm{d}^i\mathcal{T}_l(\gamma_{ls}L)}{\mathrm{d}\xi^i}=\begin{cases}(-1)^{s+i/2}\gamma_{ls}^i & i\text{ is even}\\ 0 & i\text{ is odd}\end{cases} \tag{17}$$

according to the wavenumbers defined in Eq. (8). Also, an inspection on Eq. (10) suggests the following relationships to be valid

$$p_{1km}^2+p_{2km}^2=2\alpha_{km}^2-\chi,\quad q_{1jn}^2+q_{2jn}^2=2\beta_{jn}^2-\chi, \tag{18a}$$

$$p_{2km}^2-p_{1km}^2=\sqrt{\chi^2+4\kappa},\quad q_{2jn}^2-q_{1jn}^2=\sqrt{\chi^2+4\kappa}, \tag{18b}$$

$$p_{1km}^2p_{2km}^2=\alpha_{km}^2(\alpha_{km}^2-\chi)-\kappa,\quad q_{1jn}^2q_{2jn}^2=\beta_{jn}^2(\beta_{jn}^2-\chi)-\kappa, \tag{18c}$$

$$(p_{1km}^2+\beta_{jn}^2)(p_{2km}^2+\beta_{jn}^2)=(q_{1jn}^2+\alpha_{km}^2)(q_{2jn}^2+\alpha_{km}^2). \tag{18d}$$

The above expressions will be used later.

## 3. Development of the spectral-dynamic stiffness matrix

The general solution obtained previously will serve as the frequency-dependent dynamic shape functions to develop the spectral-dynamic stiffness (S-DS) matrix in this section. In this method, the general solution $W(x,y)$ of Eq. (11) has been partitioned into four components $W^{kj}$ in Eq. (12). In this section, advantage of the above partitioning is taken by first developing the S-DS component matrix $\boldsymbol{K}^{kj}$ based on the expressions of Eq. (12). These $\boldsymbol{K}^{kj}$ matrices are then assembled to form the overall $\boldsymbol{K}$ for the entire plate. The final S-DS matrix $\boldsymbol{K}_f$ is obtained by applying the prescribed boundary conditions onto the S-DS matrix $\boldsymbol{K}$, see Section 3.2.

### 3.1. Development of the S-DS component matrix $\boldsymbol{K}^{kj}$

The formulation of the S-DS component matrices $\boldsymbol{K}^{kj}$ is achieved by substituting the general solution component of Eq. (12) into the corresponding boundary conditions and eliminating the unknown coefficients. Note that the following derivation procedure is general so that it is valid for all of the four $kj$ symmetric/antisymmetric component cases.

For the sake of brevity, the displacement and force boundary conditions on the plate edges can be written in vector form as

$$\begin{bmatrix}W_a^{kj}\\ W_b^{kj}\\ \phi_a^{kj}\\ \phi_b^{kj}\end{bmatrix},\qquad \begin{bmatrix}V_a^{kj}\\ V_b^{kj}\\ M_a^{kj}\\ M_b^{kj}\end{bmatrix}. \tag{19}$$

The entries in the above vectors ($W_a^{kj}, V_a^{kj}$, etc.) can be expressed either by substituting the solution components of Eq. (12) into the natural boundary conditions of Eq. (3) or by expressing them using the modified Fourier series of Eq. (A.2). Thus,

$$\begin{bmatrix} W_a^{kj} \\ W_b^{kj} \\ \phi_a^{kj} \\ \phi_b^{kj} \end{bmatrix} = \begin{bmatrix} W^{kj}|_{x=a} \\ W^{kj}|_{y=b} \\ -\frac{\partial W^{kj}}{\partial x}|_{x=a} \\ -\frac{\partial W^{kj}}{\partial y}|_{y=b} \end{bmatrix} = \begin{bmatrix} \sum_{n\in\mathbb{N}} W_{ajn} \frac{\mathcal{T}_j(\beta_{jn}y)}{\sqrt{\zeta_{jn}b}} \\ \sum_{m\in\mathbb{N}} W_{bkm} \frac{\mathcal{T}_k(\alpha_{km}x)}{\sqrt{\zeta_{km}a}} \\ \sum_{n\in\mathbb{N}} \phi_{ajn} \frac{\mathcal{T}_j(\beta_{jn}y)}{\sqrt{\zeta_{jn}b}} \\ \sum_{m\in\mathbb{N}} \phi_{bkm} \frac{\mathcal{T}_k(\alpha_{km}x)}{\sqrt{\zeta_{km}a}} \end{bmatrix}, \tag{20a}$$

$$\begin{bmatrix} V_a^{kj} \\ V_b^{kj} \\ M_a^{kj} \\ M_b^{kj} \end{bmatrix} = D \begin{bmatrix} -\left(\frac{\partial^3}{\partial x^3} + \Gamma^* \frac{\partial^3}{\partial x \partial y^2} + \chi \frac{\partial}{\partial x}\right) W^{kj}|_{x=a} \\ -\left(\frac{\partial^3}{\partial y^3} + \Gamma^* \frac{\partial^3}{\partial y \partial x^2} + \chi \frac{\partial}{\partial y}\right) W^{kj}|_{y=b} \\ -\left(\frac{\partial^2}{\partial x^2} + \nu \frac{\partial}{\partial y^2}\right) W^{kj}|_{x=a} \\ -\left(\frac{\partial^2}{\partial y^2} + \nu \frac{\partial^2}{\partial x^2}\right) W^{kj}|_{y=b} \end{bmatrix} = D \begin{bmatrix} \sum_{n\in\mathbb{N}} V_{ajn} \frac{\mathcal{T}_j(\beta_{jn}y)}{\sqrt{\zeta_{jn}b}} \\ \sum_{m\in\mathbb{N}} V_{bkm} \frac{\mathcal{T}_k(\alpha_{km}x)}{\sqrt{\zeta_{km}a}} \\ \sum_{n\in\mathbb{N}} M_{ajn} \frac{\mathcal{T}_j(\beta_{jn}y)}{\sqrt{\zeta_{jn}b}} \\ \sum_{m\in\mathbb{N}} M_{bkm} \frac{\mathcal{T}_k(\alpha_{km}x)}{\sqrt{\zeta_{km}a}} \end{bmatrix}, \tag{20b}$$

The modified Fourier coefficients of the boundary conditions (e.g. $W_{ajn}$ and $V_{bkm}$ in Eq. (20) were obtained from the modified Fourier series of Eq. (A.2) to give

$$W_{ajn} = \int_{-b}^{b} W_a^{kj} \frac{\mathcal{T}_j(\beta_{jn}y)}{\sqrt{\zeta_{jn}b}} \mathrm{d}y, \quad V_{bkm} = \int_{-a}^{a} \frac{V_b^{kj}}{D} \frac{\mathcal{T}_k(\alpha_{km}x)}{\sqrt{\zeta_{km}a}} \mathrm{d}x. \tag{21}$$

The $\sqrt{\zeta_{jn}b}$ and $\sqrt{\zeta_{km}a}$ appearing in Eqs. (20) and (21) provide the symmetry of the forward and inverse modified Fourier transformation to eliminate the dependence of the length in the integral ranges $[-b, b]$ or $[-a, a]$. Therefore, when $a \neq b$ the ensuing S-DS component matrices $\boldsymbol{K}^{kj}$ will remain symmetric. This is the second key step taken in the method.

In view of Eqs. (16) and (17), the expressions for $\phi_a^{kj}$ in Eq. (20a) and $V_a^{kj}$ in Eq. (20b) yield

$$-\partial W^{kj}/\partial x\big|_{x=a} = \sum_{n\in\mathbb{N}} \phi_{ajn} \mathcal{T}_j(\beta_{jn}y)/\sqrt{\zeta_{jn}b}, \tag{22a}$$

$$-\left(\frac{\partial^3}{\partial x^3} + \Gamma^* \frac{\partial^3}{\partial x \partial y^2} + \chi \frac{\partial}{\partial x}\right) W^{kj}|_{x=a} = \sum_{n\in\mathbb{N}} V_{ajn} \frac{\mathcal{T}_j(\beta_{jn}y)}{\sqrt{\zeta_{jn}b}}, \tag{22b}$$

which give

$$-\phi_{ajn}/\sqrt{\zeta_{jn}b} = q_{1jn}\mathcal{H}_k^*(q_{1jn}a)B_{1jn} + q_{2jn}\mathcal{H}_k^*(q_{2jn}a)B_{2jn}, \tag{23a}$$

$$-V_{ajn}/\sqrt{\zeta_{jn}b} = \left(q_{1jn}^2 - \Gamma^*\beta_{jn}^2 + \chi\right) q_{1jn}\mathcal{H}_k^*(q_{1jn}a)B_{1jn} + \left(q_{2jn}^2 - \Gamma^*\beta_{jn}^2 + \chi\right) q_{2jn}\mathcal{H}_k^*(q_{2jn}a)B_{2jn} \tag{23b}$$

for all $n \in \mathbb{N}$. With the help of Eq. (18a), the unknowns coefficients $B_{1jn}$ and $B_{2jn}$ can be determined from Eq. (23) for all $n \in \mathbb{N}$. These are

$$B_{1jn} = \frac{V_{ajn} - (\nu\beta_{jn}^2 - q_{1jn}^2)\phi_{ajn}}{\sqrt{\zeta_{jn}b}\sqrt{\chi^2 + 4\kappa}\, q_{1jn}\mathcal{H}_k^*(q_{1jn}a)}, \tag{24a}$$

$$B_{2jn} = -\frac{V_{ajn} - (\nu\beta_{jn}^2 - q_{2jn}^2)\phi_{ajn}}{\sqrt{\zeta_{jn}b}\sqrt{\chi^2 + 4\kappa}\, q_{2jn}\mathcal{H}_k^*(q_{2jn}a)}. \tag{24b}$$

Following similar procedure and with the help of Eq. (18a), the expressions of $\phi_b^{kj}$ in Eq. (20a) and $V_b^{kj}$ in Eq. (20b) yield the unknowns $A_{1km}$ and $A_{2km}$ as

$$A_{1km} = \frac{V_{bkm} - (\nu\alpha_{km}^2 - p_{1km}^2)\phi_{bkm}}{\sqrt{\zeta_{km}a}\sqrt{\chi^2 + 4\kappa}\, p_{1km}\mathcal{H}_j^*(p_{1km}b)}, \tag{25a}$$

$$A_{2km} = -\frac{V_{bkm} - (\nu\alpha_{km}^2 - p_{2km}^2)\phi_{bkm}}{\sqrt{\zeta_{km}a}\sqrt{\chi^2 + 4\kappa}\, p_{2km}\mathcal{H}_j^*(p_{2km}b)}. \tag{25b}$$

So far, all of the unknown coefficients $A_{1km}, A_{2km}, B_{1jn}$ and $B_{1jn}$ in the general solution of Eq. (12) have been determined by using the expressions of $\phi_a^{kj}, \phi_b^{kj}, V_a^{kj}$ and $V_b^{kj}$ of Eq. (20). Next, by substituting the already determined unknowns into the rest of the expressions for $W_a^{kj}, W_b^{kj}, M_a^{kj}$ and $M_b^{kj}$ in Eq. (20) and by applying the modified Fourier series formula (A.2), one can arrive at four infinite sets of algebraic equations relating all the Fourier coefficients ($W_{ajn}, W_{bkm}$, etc.) in Eq. (20). The detailed derivation is described in Appendix B. To this end, the four infinite sets of equations can be recast into the following vector form:

$$\begin{bmatrix} \boldsymbol{W}^{kj} \\ \boldsymbol{M}^{kj} \end{bmatrix} = \begin{bmatrix} \boldsymbol{A}_{W\Phi}^{kj} & \boldsymbol{A}_{WV}^{kj} \\ \boldsymbol{A}_{M\Phi}^{kj} & \boldsymbol{A}_{MV}^{kj} \end{bmatrix} \begin{bmatrix} \boldsymbol{\Phi}^{kj} \\ \boldsymbol{V}^{kj} \end{bmatrix} \tag{26}$$

where

$$\boldsymbol{V}^{kj} = [V_{aj0}, V_{aj1}, \ldots, V_{ajn}, \ldots, V_{bk0}, V_{bk1}, \ldots, V_{bkm}, \ldots]^T, \tag{27a}$$

$$\boldsymbol{M}^{kj} = [M_{aj0}, M_{aj1}, \ldots, M_{ajn}, \ldots, M_{bk0}, M_{bk1}, \ldots, M_{bkm}, \ldots]^T, \tag{27b}$$

$$\boldsymbol{W}^{kj} = [W_{aj0}, W_{aj1}, \ldots, W_{ajn}, \ldots, W_{bk0}, W_{bk1}, \ldots, W_{bkm}, \ldots]^T, \tag{27c}$$

$$\boldsymbol{\Phi}^{kj} = [\phi_{aj0}, \phi_{aj1}, \ldots, \phi_{ajn}, \ldots, \phi_{bk0}, \phi_{bk1}, \ldots, \phi_{bkm}, \ldots]^T. \tag{27d}$$

The explicit expressions for the coefficient matrices $\boldsymbol{A}_{W\Phi}^{kj}, \boldsymbol{A}_{WV}^{kj}, \boldsymbol{A}_{M\Phi}^{kj}$ and $\boldsymbol{A}_{MV}^{kj}$ are given in Appendix C in a remarkably concise form whose physical meanings are also interpreted. It is worth emphasising that the whole coefficient matrix of the right hand side of Eq. (26) has a symplectic structure: $\boldsymbol{A}_{WV}^{kj}$ and $\boldsymbol{A}_{M\Phi}^{kj}$ are symmetric matrices and $\boldsymbol{A}_{W\Phi}^{kj} = -\boldsymbol{A}_{MV}^{kj\,T}$. This is owing to the adoption of the modified Fourier series formula (A.2) in the formulation which keeps the symplecticity [57] of the original Hamiltonian system. On the basis of Eq. (26), the spectral-dynamic stiffness (S-DS) matrix $\boldsymbol{K}^{kj}$ can be constructed in the form

$$\boldsymbol{f}^{kj} = \boldsymbol{K}^{kj}\boldsymbol{d}^{kj}, \tag{28}$$

in which

$$\boldsymbol{f}^{kj} = D\begin{bmatrix} \boldsymbol{V}^{kj} \\ \boldsymbol{M}^{kj} \end{bmatrix}, \quad \boldsymbol{d}^{kj} = \begin{bmatrix} \boldsymbol{W}^{kj} \\ \boldsymbol{\Phi}^{kj} \end{bmatrix},$$
$$\boldsymbol{K}^{kj} = D\begin{bmatrix} \boldsymbol{A}_{WV}^{kj\,-1} & -\boldsymbol{A}_{WV}^{kj\,-1}\boldsymbol{A}_{W\Phi}^{kj} \\ \boldsymbol{A}_{MV}^{kj}\boldsymbol{A}_{WV}^{kj\,-1} & \boldsymbol{A}_{M\Phi}^{kj} - \boldsymbol{A}_{MV}^{kj}\boldsymbol{A}_{WV}^{kj\,-1}\boldsymbol{A}_{W\Phi}^{kj} \end{bmatrix}. \tag{29}$$

In the above equation, the scalar parameter $D$ is the plate rigidity (recalling the $D$ in Eq. (20b)).

### 3.2. Assembly procedure using the S-DS component matrix $\boldsymbol{K}^{kj}$ to form the complete S-DS matrix $\boldsymbol{K}$

In this section, the previously formulated S-DS component matrix $\boldsymbol{K}^{kj}$ for the four symmetric or anti-symmetric component cases are to be assembled to form the S-DS matrix $\boldsymbol{K}$ of the entire plate.

Using the modified Fourier series formula of Eq. (A.2), any arbitrarily prescribed boundary conditions on the four plate boundaries can be transformed into the vector form $\boldsymbol{d}$ and $\boldsymbol{f}$ as

$$\boldsymbol{d} = \left[\boldsymbol{d}_1^T, \boldsymbol{d}_2^T, \boldsymbol{d}_3^T, \boldsymbol{d}_4^T\right]^T, \quad \boldsymbol{f} = \left[\boldsymbol{f}_1^T, \boldsymbol{f}_2^T, \boldsymbol{f}_3^T, \boldsymbol{f}_4^T\right]^T, \tag{30}$$

in which

$$\boldsymbol{d}_i = \left[\boldsymbol{W}_i^{0T}, \boldsymbol{W}_i^{1T}, \boldsymbol{\Phi}_i^{0T}, \boldsymbol{\Phi}_i^{1T}\right]^T, \quad \boldsymbol{f}_i = \left[\boldsymbol{V}_i^{0T}, \boldsymbol{V}_i^{1T}, \boldsymbol{M}_i^{0T}, \boldsymbol{M}_i^{1T}\right]^T, \tag{31}$$

where the sub-vectors superscripted by '0' and '1' denote respectively the vectors of the Fourier cosine and sine series coefficients. Following the partition of the general solution into four components as shown in Eq. (11), the displacement and force vectors $\boldsymbol{d}$ and $\boldsymbol{f}$ in Eq. (30) can be split into four symmetric or anti-symmetric components. Therefore, the combination of the four sub-vectors in each case represents the total displacement and force vectors on the boundaries of the plate. In this way, one can write

$$\boldsymbol{d} = \boldsymbol{T}[\boldsymbol{d}^{00^T}, \boldsymbol{d}^{01^T}, \boldsymbol{d}^{10^T}, \boldsymbol{d}^{11^T}]^T, \quad \boldsymbol{f} = \boldsymbol{T}[\boldsymbol{f}^{00^T}, \boldsymbol{f}^{01^T}, \boldsymbol{f}^{10^T}, \boldsymbol{f}^{11^T}]^T, \tag{32}$$

where $\boldsymbol{T}$ is the total transfer matrix taking the form

$$\boldsymbol{T} = \begin{bmatrix}
\boldsymbol{I}_n & \boldsymbol{O} & \boldsymbol{O} & \boldsymbol{O} & \boldsymbol{O} & \boldsymbol{O} & \boldsymbol{O} & \boldsymbol{O} & \boldsymbol{I}_n & \boldsymbol{O} & \boldsymbol{O} & \boldsymbol{O} & \boldsymbol{O} & \boldsymbol{O} & \boldsymbol{O} & \boldsymbol{O} \\
\boldsymbol{O} & \boldsymbol{O} & \boldsymbol{O} & \boldsymbol{O} & \boldsymbol{I}_n & \boldsymbol{O} & \boldsymbol{O} & \boldsymbol{O} & \boldsymbol{O} & \boldsymbol{O} & \boldsymbol{O} & \boldsymbol{O} & \boldsymbol{I}_n & \boldsymbol{O} & \boldsymbol{O} & \boldsymbol{O} \\
\boldsymbol{O} & \boldsymbol{I}_n & \boldsymbol{O} & \boldsymbol{O} & \boldsymbol{O} & \boldsymbol{O} & \boldsymbol{O} & \boldsymbol{O} & \boldsymbol{O} & \boldsymbol{I}_n & \boldsymbol{O} & \boldsymbol{O} & \boldsymbol{O} & \boldsymbol{O} & \boldsymbol{O} & \boldsymbol{O} \\
\boldsymbol{O} & \boldsymbol{O} & \boldsymbol{O} & \boldsymbol{O} & \boldsymbol{O} & \boldsymbol{I}_n & \boldsymbol{O} & \boldsymbol{O} & \boldsymbol{O} & \boldsymbol{O} & \boldsymbol{O} & \boldsymbol{O} & \boldsymbol{O} & \boldsymbol{I}_n & \boldsymbol{O} & \boldsymbol{O} \\
\boldsymbol{O} & \boldsymbol{O} & \boldsymbol{I}_m & \boldsymbol{O} & \boldsymbol{O} & \boldsymbol{O} & \boldsymbol{I}_m & \boldsymbol{O} & \boldsymbol{O} & \boldsymbol{O} & \boldsymbol{O} & \boldsymbol{O} & \boldsymbol{O} & \boldsymbol{O} & \boldsymbol{O} & \boldsymbol{O} \\
\boldsymbol{O} & \boldsymbol{O} & \boldsymbol{O} & \boldsymbol{O} & \boldsymbol{O} & \boldsymbol{O} & \boldsymbol{O} & \boldsymbol{O} & \boldsymbol{O} & \boldsymbol{O} & \boldsymbol{I}_m & \boldsymbol{O} & \boldsymbol{O} & \boldsymbol{O} & \boldsymbol{I}_m & \boldsymbol{O} \\
\boldsymbol{O} & \boldsymbol{O} & \boldsymbol{O} & \boldsymbol{I}_m & \boldsymbol{O} & \boldsymbol{O} & \boldsymbol{O} & \boldsymbol{I}_m & \boldsymbol{O} & \boldsymbol{O} & \boldsymbol{O} & \boldsymbol{O} & \boldsymbol{O} & \boldsymbol{O} & \boldsymbol{O} & \boldsymbol{O} \\
\boldsymbol{O} & \boldsymbol{O} & \boldsymbol{O} & \boldsymbol{O} & \boldsymbol{O} & \boldsymbol{O} & \boldsymbol{O} & \boldsymbol{O} & \boldsymbol{O} & \boldsymbol{O} & \boldsymbol{O} & \boldsymbol{I}_m & \boldsymbol{O} & \boldsymbol{O} & \boldsymbol{O} & \boldsymbol{I}_m \\
\boldsymbol{I}_n & \boldsymbol{O} & \boldsymbol{O} & \boldsymbol{O} & \boldsymbol{O} & \boldsymbol{O} & \boldsymbol{O} & \boldsymbol{O} & -\boldsymbol{I}_n & \boldsymbol{O} & \boldsymbol{O} & \boldsymbol{O} & \boldsymbol{O} & \boldsymbol{O} & \boldsymbol{O} & \boldsymbol{O} \\
\boldsymbol{O} & \boldsymbol{O} & \boldsymbol{O} & \boldsymbol{O} & \boldsymbol{I}_n & \boldsymbol{O} & \boldsymbol{O} & \boldsymbol{O} & \boldsymbol{O} & \boldsymbol{O} & \boldsymbol{O} & \boldsymbol{O} & -\boldsymbol{I}_n & \boldsymbol{O} & \boldsymbol{O} & \boldsymbol{O} \\
\boldsymbol{O} & -\boldsymbol{I}_n & \boldsymbol{O} & \boldsymbol{O} & \boldsymbol{O} & \boldsymbol{O} & \boldsymbol{O} & \boldsymbol{O} & \boldsymbol{O} & \boldsymbol{I}_n & \boldsymbol{O} & \boldsymbol{O} & \boldsymbol{O} & \boldsymbol{O} & \boldsymbol{O} & \boldsymbol{O} \\
\boldsymbol{O} & \boldsymbol{O} & \boldsymbol{O} & \boldsymbol{O} & \boldsymbol{O} & -\boldsymbol{I}_n & \boldsymbol{O} & \boldsymbol{O} & \boldsymbol{O} & \boldsymbol{O} & \boldsymbol{O} & \boldsymbol{O} & \boldsymbol{O} & \boldsymbol{I}_n & \boldsymbol{O} & \boldsymbol{O} \\
\boldsymbol{O} & \boldsymbol{O} & \boldsymbol{I}_m & \boldsymbol{O} & \boldsymbol{O} & \boldsymbol{O} & -\boldsymbol{I}_m & \boldsymbol{O} & \boldsymbol{O} & \boldsymbol{O} & \boldsymbol{O} & \boldsymbol{O} & \boldsymbol{O} & \boldsymbol{O} & \boldsymbol{O} & \boldsymbol{O} \\
\boldsymbol{O} & \boldsymbol{O} & \boldsymbol{O} & \boldsymbol{O} & \boldsymbol{O} & \boldsymbol{O} & \boldsymbol{O} & \boldsymbol{O} & \boldsymbol{O} & \boldsymbol{O} & \boldsymbol{I}_m & \boldsymbol{O} & \boldsymbol{O} & \boldsymbol{O} & -\boldsymbol{I}_m & \boldsymbol{O} \\
\boldsymbol{O} & \boldsymbol{O} & \boldsymbol{O} & -\boldsymbol{I}_m & \boldsymbol{O} & \boldsymbol{O} & \boldsymbol{O} & \boldsymbol{I}_m & \boldsymbol{O} & \boldsymbol{O} & \boldsymbol{O} & \boldsymbol{O} & \boldsymbol{O} & \boldsymbol{O} & \boldsymbol{O} & \boldsymbol{O} \\
\boldsymbol{O} & \boldsymbol{O} & \boldsymbol{O} & \boldsymbol{O} & \boldsymbol{O} & \boldsymbol{O} & \boldsymbol{O} & \boldsymbol{O} & \boldsymbol{O} & \boldsymbol{O} & -\boldsymbol{I}_m & \boldsymbol{O} & \boldsymbol{O} & \boldsymbol{O} & \boldsymbol{I}_m
\end{bmatrix}, \tag{33}$$

Here $\boldsymbol{I}_n$ and $\boldsymbol{I}_m$ are identity matrices of dimension $n$ and $m$ respectively, and $\boldsymbol{O}$ represents null matrices. It is interesting to note that $\boldsymbol{T}$ has the following property

$$\boldsymbol{T}^{-1} = \boldsymbol{T}^T/2, \quad \forall\, M, N \in \mathbb{N}. \tag{34}$$

Applying the property shown in Eq. (34) to Eq. (32) yields

$$[\boldsymbol{d}^{00^T}, \boldsymbol{d}^{01^T}, \boldsymbol{d}^{10^T}, \boldsymbol{d}^{11^T}]^T = \frac{1}{2}\boldsymbol{T}^T\boldsymbol{d}. \tag{35}$$

Finally, putting Eqs. (28), (30), (32) and (35) together leads to the relation:

$$\boldsymbol{f} = \boldsymbol{K}\boldsymbol{d}, \tag{36}$$

where

$$\boldsymbol{K} = \frac{1}{2}\boldsymbol{T}\begin{bmatrix} \boldsymbol{K}^{00} & \boldsymbol{O} & \boldsymbol{O} & \boldsymbol{O} \\ \boldsymbol{O} & \boldsymbol{K}^{01} & \boldsymbol{O} & \boldsymbol{O} \\ \boldsymbol{O} & \boldsymbol{O} & \boldsymbol{K}^{10} & \boldsymbol{O} \\ \boldsymbol{O} & \boldsymbol{O} & \boldsymbol{O} & \boldsymbol{K}^{11} \end{bmatrix}\boldsymbol{T}^T. \tag{37}$$

In Eq. (36), $\boldsymbol{K}$ is the S-DS matrix for the entire plate, which relates the force $\boldsymbol{f}$ and displacement $\boldsymbol{d}$ vectors on the four edges of the plate. Each element of $\boldsymbol{f}$ or $\boldsymbol{d}$ corresponds to a frequency-wavenumber dependent DOF on the plate boundary (FWDOF). Finally, any arbitrarily prescribed boundary conditions on the four plate edges can be transformed into vectors in the form of Eqs. (30) and (31). The zero elements, if any, in the vector $\boldsymbol{d}$ will be removed yielding $\boldsymbol{d}_f$ and the corresponding rows and columns of $\boldsymbol{K}$ will be condensed leading to $\boldsymbol{K}_f$, and $\boldsymbol{f}$ reduced to $\boldsymbol{f}_f$.

## 4. The Wittrick–Williams algorithm and its enhancements

The final spectral-dynamic stiffness (S-DS) matrix $\boldsymbol{K}_f$ for a plate with arbitrarily prescribed boundary conditions can now be used to perform an accurate and efficient free vibration analysis. A reliable method of computing the natural frequencies of a structure using the S-DS method is to apply the well-known Wittrick–Williams (WW) algorithm [47]. Essentially, the algorithm monitors the Sturm sequence condition of $\boldsymbol{K}_f$ in such a way that there is no possibility of missing any natural frequency of the structure. Moreover, any required natural frequency can be computed to any desired precision even from only a single element.

In the Wittrick–Williams algorithm, the mode count $J$ is a fundamental concept, which defines the number of natural frequencies passed as the frequency $\omega$ is increased from zero to $\omega^*$. The mode count $J$ is given by

$$J = J_0 + s\{\boldsymbol{K}_f\}, \tag{38}$$

where $\boldsymbol{K}_f$, whose elements all depend on $\omega$, is evaluated at $\omega = \omega^*$; $s\{\boldsymbol{K}_f\}$ is the number of negative elements on the leading diagonal of $\boldsymbol{K}_f^\Delta$ and $\boldsymbol{K}_f^\Delta$ is the upper triangular matrix obtained by applying the Gauss elimination to $\boldsymbol{K}_f$; $J_0$ is the number of natural frequencies between $\omega = 0$ and $\omega = \omega^*$ for the plate with all its ends clamped, namely when $\boldsymbol{d} = \boldsymbol{0}$. Thus, it is possible to ascertain how many natural frequencies of a structure lie below an arbitrarily chosen trial frequency $\omega^*$. This simple feature of the algorithm (coupled with the fact that successive trial frequencies can be chosen by the user to bracket a natural frequency) can be used to converge on any required natural frequency to any desired accuracy.

It is apparent from above that $J_0$ count is an essential part of the algorithm, not a peripheral issue. However, computation of $J_0$ can sometimes be a difficult task and may become a drawback when applying the algorithm. In the literature, many of the previous DS methods on plates [49–53] used a sufficiently fine mesh to ensure that $J_0 \equiv 0$ at the frequency range of interest. However, this will no doubt increase the computation time. It is especially the case for the current S-DSM because a finer mesh will increase the number of DOFs more significantly than that in the DS theory of a Levy-type plate. However, there is another strategy to compute $J_0$ indirectly by considering the Navier type plate whose edges are all simply supported. Obviously, Eq. (38) also applies to such a special case, i.e., for a trial frequency $\omega^*$, one has $J_S = J_0 + s\{\boldsymbol{K}_S\}$, where $J_S$ is the overall mode count of the Navier plate, and $s(\boldsymbol{K}_S)$ is the sign count of the formulated S-DS matrix $\boldsymbol{K}_S$ of the Navier plate. Therefore, the $J_0$ can be obtained indirectly as below

$$J_0 = J_S - s(\boldsymbol{K}_S). \tag{39}$$

Similar technique as that of Eq. (39) has been successfully applied to beam elements [58,59]. However, when it comes to plate problems it becomes more complicated. In fact, this technique has been restricted to the most simple Levy case when the corresponding DS matrix $\boldsymbol{K}_S$ can be decoupled into $2 \times 2$ matrices. The technique of Eq. (39) has never been applied so far for cases when the corresponding DS matrices $\boldsymbol{K}_S$ are more complex, see e.g., [48–53]. To meet this challenge, a set of novel techniques is proposed here to compute $J_0$ in an extremely efficient and robust way.

First the computation of $J_S$ in Eq. (39) is accomplished analytically in the light of the knowledge in analytical number theory. It is well-known that the exact solution for the natural frequency of an all-round simply supported Kirchhoff plate is the familiar Navier solution [56]. The dimensionless natural frequency parameter for this case can be expressed analytically in the following form

$$\left(\frac{2a}{\pi}\right)^2\sqrt{\frac{\rho h}{D}}\omega_{\hat{m}\hat{n}} = \frac{\hat{m}^2 + (\hat{n}a/b)^2}{1 + (\pi h/a)^2\left[\hat{m}^2 + (\hat{n}a/b)^2\right]/48}, \tag{40}$$

where $\hat{m}$ and $\hat{n}$ are the number of half-waves in the $x$ and $y$ direction respectively ($\hat{m}$ and $\hat{n}$ are used to distinguish with previous $m$ and $n$, the number of terms in the series expansion). Then, $J_S$ of Eq. (39) is essentially the number of pairs of $\hat{m}$ and $\hat{n}$ such that the left-hand side of Eq. (40) with $\omega_{\hat{m}\hat{n}} = \omega^*$ is greater than the right-hand side. Obviously, this can be implemented using a numerical search technique which can be computationally expensive and the procedure may possibly miss some of the natural frequencies. However, there indeed exists an analytical expression for determining $J_S$ if one recognises that this problem is an extension of the analytical number theory problem called *Gauss circle problem* [60]. Thus, $J_S$ can be given as follows

$$J_S = \sum_{\hat{n}=1}^{\lfloor \sqrt[4]{\Pi_1} \rfloor} \lfloor \hat{m}^*(\hat{n}, \omega^*) \rfloor, \tag{41}$$

in which

$$\hat{m}^*(\hat{n}, \omega^*) = \sqrt{\left[\Pi_2 + \sqrt{\Pi_2^2 + 4\Pi_1}\right]/2 - (\hat{n}a/b)^2}, \tag{42}$$

$$\Pi_1 = (2a/\pi)^4 \omega^{*2} \rho h/D, \Pi_2 = (\omega^* a/\pi)^2 \rho h^3/(3D). \tag{43}$$

In Eq (41), '$\lfloor \cdot \rfloor$' is the floor function denoting the largest integer not greater than '$\cdot$'. The detailed mathematical proof is not given here for the sake of brevity.

The computation of $s(\boldsymbol{K}_S)$ in Eq. (39) is achieved in an elegant and efficient way by taking advantage of the symplecticity of the coefficient matrices in Eq. (26). It is well-known that when a geometrically symmetric structure is subject to symmetric boundary conditions, the displacement field is either symmetric or antisymmetric. Therefore, when a rectangular plate subjected to simple supports on all its edges, the four symmetric/antisymmetric S-DS matrices are decoupled to describe the deformation with corresponding symmetric/antisymmetric properties. Hence,

$$s(\boldsymbol{K}_S) = \sum_{k,j \in \{0,1\}} s(\boldsymbol{K}_S^{kj}). \tag{44}$$

Now returning to Eq. (28), the case with all the plate edges simply supported is equivalent to letting $\boldsymbol{M}^{kj} = \boldsymbol{W}^{kj} = \boldsymbol{0}$, so that $s(\boldsymbol{K}_S^{kj}) = s(\boldsymbol{A}_{M\Phi}^{kj} - \boldsymbol{A}_{MV}^{kj} {\boldsymbol{A}_{WV}^{kj}}^{-1} \boldsymbol{A}_{W\Phi}^{kj})$. Thus

$$s(\boldsymbol{K}_S) = \sum_{k,j \in \{0,1\}} s(\boldsymbol{A}_{M\Phi}^{kj} - \boldsymbol{A}_{MV}^{kj} {\boldsymbol{A}_{WV}^{kj}}^{-1} \boldsymbol{A}_{W\Phi}^{kj}). \tag{45}$$

The above technique of computing $J_S$ and $s(\boldsymbol{K}_S)$ retains high reliability and accuracy of the WW algorithm application by providing the $J_0$ in an elegant and extremely efficient way.

The mode shape computation is a little bit more complicated than that of the usual procedure generally adopted in other DSM methods. Once an arbitrary value is assigned to a chosen degree of freedom, the rest of the values in the displacement vector $\boldsymbol{d}_f$ can be determined in terms of the given one by solving the algebraic system. Then the displacement component vectors $\boldsymbol{d}^{kj}$ can be determined from $\boldsymbol{d}$ by using Eq. (35). Subsequently $\boldsymbol{f}^{kj}$ can be obtained from Eq. (28). Finally the unknown coefficients can be calculated using Eqs. (24) and (25) which will be substituted into Eq. (12) to recover the mode shapes.

## 5. Results

The current S-DSM has been implemented into a MATLAB program which computes the natural frequencies and mode shapes of rectangular plates with arbitrary boundary conditions. To keep the presentation concise, selective but representative examples are presented in this section. The results computed by the present S-DSM are accurate up to the last figure presented which is rounded (all accurate values are shown in bold). Six or seven digit accuracy is provided to establish benchmark solutions. Some of these results are compared with published ones wherever possible to facilitate discussions on a wide range of different analytical methods for free vibration analysis of plates, see Section 6. Some representative mode shapes computed by the S-DSM are also presented.

Attention should be paid that the dimensions of the plate are always $2a \times 2b$ and the dimensionless frequency parameters are defined accordingly when the results are presented.

### 5.1. Convergence, boundedness and efficiency studies

Of course, by using the current method, any desired accuracy of results can be achieved by using suitable number of terms in the series expansion. However, the series-form general solution of Eq. (12) and the resultant infinite algebraic systems of Eq. (28) will have to be truncated at some stage during the numerical computation. Therefore, the convergence rate and the computational efficiency of this method should be properly examined. For this purpose, extensive case studies have been performed to examine the high convergence rate as well as the high efficiency of the current method.

Table 1 shows four sets of results for a square plate with different boundary conditions, namely, FFFF, CCCC, CCSC and SCSC. Throughout this paper, F, C and S represent free, clamped and simply supported edges of the plate respectively. The first, second, third and fourth letters of each four-letter combination are for the right, up, left and bottom edges respectively in an anticlockwise sense. The first eight dimensionless natural frequencies $\lambda = 4\omega a^2\sqrt{\rho h/D}$ are computed by the current S-DSM when $M = N$, the number of terms in the series, varies from 2 to 20. The results are compared with those obtained by FEM package ABAQUS using a very fine mesh with $300 \times 300$ S4R5 elements (four-node thin shell elements with five DOFs at each node). The plate parameters in the FEM modelling are taken as $2a = 2b = 1$ m, $h = 0.001$ m, $E = 30$ GPa, $\nu = 0.3$, $\rho = 2500$ kN/m$^3$. For the SCSC case, exact solutions from Ref. [15] are also presented which coincide with the S-DSM results. The computation of both S-DSM and FEM results was performed on a PC equipped with a 3.40 GHz Intel 4-core processor and 8 GB of memory. The total execution time for the first eight non-zeros natural frequencies is included in the last column of Table 1.

Indeed, the S-DSM results exhibit a very fast convergence rate relating to the number of series terms. With only 2–3 terms included in the series, the first eight natural frequencies show three to four significant figure accuracy; a five-term series leads to five significant-figure accuracy and a fifteen-term series gives results with accuracy of at least six significant figures. This is indeed an extremely fast convergence rate compared with other series based methods. For example, Ref. [61] gives only two digit accuracy results for an FFFF plate with 30 terms in the series, Ref. [11] gives five-digit precision in the results for the first six natural frequencies of a CCCC plate with at least 17 terms included in the series. Numerical studies also indicate that the convergence rate is slightly different for different BC, which is not unexpected. To obtain results with the same level of accuracy, the cases with the same prescribed BC on all edges like FFFF and CCCC require less terms in the series than the other cases like CCSC and SCSC. Nevertheless, for all of the cases, the convergence rate is seemingly much faster than all existing methods.

Although the S-DSM solutions converge very fast towards exact solutions, it is worth pointing out that the boundedness of its results is quite similar to strong-formed based method like Gorman's superposition method (GSM) [7]. The boundedness of both S-DSM and GSM are case dependent. This is different from weak-form based methods like the Ritz and Kantorovich methods, whose results always serve as the upper bound of the accurate solution. Convergence studies suggest that the results of the present S-DSM converge from below if the truncated-series building blocks have more flexible boundary conditions (BC) than the original BC, such as for the CCCC case in Table 1. On the contrary, the results from S-DSM converge from above if its building blocks for the boundary conditions are stiffer than the original boundary conditions, such as the FFFF case in Table 1. However, the boundedness cannot be predicted if the building blocks contain both stiffer and

**Table 1**
Convergence, boundedness and efficiency studies for the dimensionless natural frequency parameter of a square isotropic plate ($\nu = 0.3$) with four sets of different boundary conditions using S-DSM. FEM solutions are obtained by (ABAQUS) using a 300 × 300 mesh. Exact solutions indicate the Levy solutions for SCSC case [15]. Bold values are those for which the computed eignfrequencies using S-DSM converge to the last figure of the presented values.

| $M = N$ | $\lambda = 4\omega a^2\sqrt{\rho h/D}$ | | | | | | | | Time (s) |
|---|---|---|---|---|---|---|---|---|---|
| FFFF | 4 | 5 | 6 | 7 | 8 | 9 | 10 | 11 | |
| 2 | 13.4688 | **19.5961** | 24.2708 | 34.8070 | 34.8070 | 61.0947 | 61.0947 | 63.7187 | 0.08 |
| 5 | **13.4682** | **19.5961** | **24.2702** | 34.8010 | 34.8010 | 61.0933 | 61.0933 | 63.6869 | 0.11 |
| 10 | **13.4682** | **19.5961** | **24.2702** | **34.8009** | **34.8009** | **61.0932** | **61.0932** | **63.6861** | 0.11 |
| 15 | **13.4682** | **19.5961** | **24.2702** | **34.8009** | **34.8009** | **61.0932** | **61.0932** | **63.6861** | 0.12 |
| 20 | **13.4682** | **19.5961** | **24.2702** | **34.8009** | **34.8009** | **61.0932** | **61.0932** | **63.6861** | 0.13 |
| FEM | 13.467 | 19.596 | 24.271 | 34.799 | 34.799 | 61.095 | 61.095 | 63.684 | 50.0 |
| CCCC | 1 | 2 | 3 | 4 | 5 | 6 | 7 | 8 | |
| 2 | 35.9825 | 73.3731 | 73.3731 | 108.140 | 131.159 | 131.159 | 164.386 | 164.386 | 0.08 |
| 5 | 35.9848 | 73.3932 | 73.3932 | 108.215 | **131.581** | 132.203 | 164.998 | 164.998 | 0.09 |
| 10 | **35.9852** | **73.3938** | **73.3938** | 108.216 | **131.581** | **132.205** | **165.000** | **165.000** | 0.10 |
| 15 | **35.9852** | **73.3938** | **73.3938** | **108.217** | **131.581** | **132.205** | **165.000** | **165.000** | 0.10 |
| 20 | **35.9852** | **73.3938** | **73.3938** | **108.217** | **131.581** | **132.205** | **165.000** | **165.000** | 0.11 |
| FEM | 35.985 | 73.400 | 73.400 | 108.22 | 131.59 | 132.22 | 165.01 | 165.01 | 43.0 |
| CCSC | 1 | 2 | 3 | 4 | 5 | 6 | 7 | 8 | |
| 3 | 31.8235 | 63.3170 | 71.0710 | 100.764 | 116.309 | 130.306 | 151.760 | 159.286 | 0.29 |
| 5 | 31.8258 | 63.3299 | 71.0758 | 100.790 | 116.355 | 130.350 | 151.888 | 159.470 | 0.31 |
| 10 | **31.8260** | 63.3307 | 71.0762 | **100.792** | **116.357** | **130.351** | **151.893** | 159.476 | 0.45 |
| 15 | **31.8260** | **63.3308** | **71.0763** | **100.792** | **116.357** | **130.351** | **151.893** | **159.477** | 0.70 |
| 20 | **31.8260** | **63.3308** | **71.0763** | **100.792** | **116.357** | **130.351** | **151.893** | **159.477** | 1.14 |
| FEM | 31.826 | 63.330 | 71.080 | 100.80 | 116.37 | 130.36 | 151.90 | 159.49 | 40.0 |
| SCSC | 1 | 2 | 3 | 4 | 5 | 6 | 7 | 8 | |
| 3 | 28.9482 | 54.7287 | 69.3193 | 94.5498 | 102.139 | 129.026 | 140.008 | 154.503 | 0.27 |
| 5 | 28.9508 | 54.7425 | 69.3267 | 94.5835 | 102.214 | 129.094 | 140.197 | 154.767 | 0.34 |
| 10 | 28.9508 | **54.7431** | **69.3270** | 94.5852 | **102.216** | **129.096** | 140.204 | **154.776** | 0.46 |
| 15 | **28.9509** | **54.7431** | **69.3270** | **94.5853** | **102.216** | **129.096** | **140.205** | **154.776** | 0.71 |
| 20 | **28.9509** | **54.7431** | **69.3270** | **94.5853** | **102.216** | **129.096** | **140.205** | **154.776** | 1.16 |
| FEM | 28.951 | 54.744 | 69.330 | 94.588 | 102.22 | 129.11 | 140.21 | 154.79 | 38.0 |
| Exact | 28.9509 | 54.7431 | 69.327 | 94.5853 | 102.216 | 129.096 | 140.205 | 154.776 | – |

more flexible boundary conditions with respect to the modelled plate, such as the CFFF case. These findings coincide with those of GSM as pointed out by Mochida [62]. This is due to the similarities in the adopted series and bearing in mind that both S-DSM and GSM are based on strong formulation. In any case, the aforementioned boundedness properties are not of any major consequence due to the highly accurate results presented (accurate up to all figures presented).

Moreover, results of Table 1 demonstrate enormously high computational efficiency of the current S-DSM over that of the FEM using ABAQUS. To compute the first eight natural frequencies, FEM took 38–50 s of CPU time giving results with four significant figures whereas S-DSM took only 0.09–0.34 s with five significant figures ($M = N = 5$). That is to say, S-DSM gives much more accurate results than FEM with the execution time less than 1% of its opponent (more than 100 folds advantage in computational speed).

### 5.2. Comparisons with Levy solutions and discussions on the effect of the rotatory inertia

It is well-known that exact solutions for plates are generally available for Levy-type plates (with Navier solution as a special case). Thus, it is appropriate to validate the current S-DSM with Levy solutions. The rotatory inertia effect has been included in conjunction with the CPT in the current S-DSM development, which enables discussions on the rotatory inertia effect on the free vibration of plates. In Table 2, six Levy-type cases together with an FFFF and a CCCC cases are considered. The results computed by S-DSM with/without rotatory inertia $I_2$ are compared with the exact Levy solutions without considering $I_2$ [63,44]. It can be found that the dimensionless natural frequencies of CPT without rotatory inertia calculated using S-DSM are in exact agreement with the exact Levy solutions for all of the six cases. The presence of the rotatory inertia decreases the natural frequencies to some extent as expected. The differences in results depend on the thickness of the plate as well as on the boundary conditions: The thicker is the plate, the lower the dimensionless natural frequencies will be. Also, it can be observed that the effect of rotatory inertia plays a more pronounced role for plates with clamped edges than those with free edges. However, if the rotatory inertia is not taken into consideration, the thickness of the plate will not affect the results. This is because the thickness has been rescaled out of the GDE and BC. In all of the following results, the rotatory inertia will not be taken into account.

### 5.3. Completely free and fully clamped rectangular plates

Both completely free and fully clamped plates are probably the most demanding cases which have been attempted using a wide range of different methods in the past [15]. Therefore, these two cases provide an ideal opportunity to compare the current S-DSM with other methods.

#### 5.3.1. Completely free case

The free vibration of a plate with completely free edges is probably the most historic problem firstly raised by Chladni [1]. This problem has directly motivated the development of the well-known Rayleigh [2] and Ritz [3] methods, both of which of course, fall within weak-form-based methods as mentioned earlier in Section 1. It should be noted that there are different versions of Ritz methods with admissible functions taking, for example beam characteristic [3,15] or orthogonal polynomials [64]. However, as pointed out by Leissa [15], for the completely free case, the Ritz method gives relatively poor results compared to other boundary conditions. This is due to the difficulties involved in obtaining the solution which satisfies both the GDE and the free BC. In comparison, strong-form based methods for completely free plates give much better results, including Gorman's superposition method

**Table 2**
Comparisons of the present S-DSM results using CPT with/without rotatory inertia to Levy solutions [44,63] without rotatory inertia for dimensionless natural frequency parameter $\lambda = 2\omega a^2/\pi\sqrt{\rho h/D}$ of rectangular plates ($\nu = 0.3$).

| BC | $b/a$ | Mode | CPT without $I_2$ | | **S-DSM (CPT+$I_2$)** | | |
|---|---|---|---|---|---|---|---|
| | | | Exact Levy [44,63] | **S-DSM** | $h/b$ | | |
| | | | | | 0.02 | 0.01 | 0.005 |
| SSSS | 2 | 1st | 1.963495 | **1.963495** | **1.961883** | **1.963092** | **1.963395** |
| SCSC | 1 | 7th | 22.31424 | **22.31424** | **22.26502** | **22.30190** | **22.31115** |
| SSSC | 0.5 | 4th | 32.89686 | **32.89686** | **32.86932** | **32.88996** | **32.89513** |
| SSSF | 2 | 4th | 5.908996 | **5.908996** | **5.892135** | **5.904767** | **5.907938** |
| SCSF | 1 | 3rd | 6.637068 | **6.637068** | **6.632315** | **6.635878** | **6.636770** |
| SFSF | 0.5 | 8th | 23.38027 | **23.38027** | **23.35777** | **23.37464** | **23.37886** |
| FFFF | 1 | 7th | – | **5.538734** | **5.533302** | **5.537374** | **5.538734** |
| CCCC | 1 | 5th | – | **20.94173** | **20.90330** | **20.93210** | **20.93932** |

(GSM) [7,65], the generalised Koialovich's limitant theory based on superposition method [10] and the current S-DSM. Tables 3 and 4 show the natural frequencies obtained by the present method and other methods [3,10,15,29,61,64,65].

Table 3 includes the first 41 natural frequencies in terms of the dimensionless parameter $\omega^2\rho ha^4/D$ computed by the current S-DSM, the Ritz method [3] as well as generalised Koialovich's limitant theory based on superposition method [10]. It should be emphasised that the first three modes have zero frequencies corresponding to rigid body modes: one for transverse translation and two for rotation. These three rigid body modes were not obtainable by most of the other analytical methods like Ritz [15] and superposition [65] method. However, they can be found by the current S-DSM due to the application of the Wittrick–Williams algorithm. Table 3 includes only nonzero natural frequencies starting from the fourth one. All of the first 41 natural frequencies obtained by the current S-DSM converge to the sixth digit when even less than 20 terms are used in the series. The results obtained by Ritz [3] more than a century ago are still reasonably accurate for lower frequencies, but his results deteriorate for higher natural frequencies, say, over the tenth one. The reason for this will be explained later in Section 6. The results obtained by the generalised Koialovich's limitant theory based on superposition method [10] are more accurate than the Ritz method. However, it seems that the complexities of the limitant theory method prevents the pursuit of more accurate results in a simple manner. Some representative mode shapes from the current method are presented in Fig. 2, which resemble the well-known Chaldni patterns [1]. The 5th and 39th modes are doubly symmetric, the 4th and 35th modes are doubly antisymmetric, and the 7th and 40th modes are symmetric about the $x$-axis but antisymmetric about the $y$-axis.

Table 4 compares the current method with several other methods [15,29,64,61,65]. The results are presented for different plate aspect ratios and Poisson ratios in terms of two different dimensionless natural frequency parameters $\lambda$. Note that all of the results by the current S-DSM in Table 4 are accurate up to six significant digits with only ten terms included in the series (This appears to be the most accurate results reported for FFFF case so far). The results obtained by Gorman's superposition method [65] using 15 series terms have four digit accuracy, which agree with the first four digits of the current method, see the first top half of Table 4. In the second half of Table 4, the current method is compared with four weak-form based methods, namely, three Ritz methods using different admissible functions (a set of trigonometric functions and polynomials [29], algebraic polynomials [64] and beam characteristic functions [15]) and one variational method called WEM [61]. Apart from the current S-DSM, the results by the Ritz methods in Refs. [29,64] are more accurate than the other two weak-form based methods [15,61]. The results by WEM using 30 terms in the series have only three digit precision, whose convergence rate appears to be the slowest amongst all of the other methods. Another argument on Gorman's superposition method [65] made by Rosales and Filipich in Ref. [66] appears to be in error. As claimed by Rosales and Filipich, the second frequency of an isotropic square plate (doubly symmetric, quoted as 19.61) was missing therefore it was concluded that the series functions in Ref. [65] was

**Table 3**
Dimensionless nonzero natural frequency parameters $\lambda = \omega^2\rho ha^4/D$ for a square F-F-F-F plates compared with the analytical results firstly obtained by Ritz in 1909 [3] and those using generalised Koialovich's Limitant theory by Meleshko and Papkov [10] ($\nu = 0.225$).

| Mode no. | $(k,j)$ | **S-DSM** | Limitant [10] | Ritz [3] | Mode no. | $(k,j)$ | **S-DSM** | Limitant [10] | Ritz [3] |
|---|---|---|---|---|---|---|---|---|---|
| 4 | (1, 1) | **12.4540** | 12.454 | 12.43 | 23 | (0, 1) | **2476.92** | 2476.9 | 2500 |
| 5 | (0, 0) | **25.9764** | 25.949 | 26.40 | 24 | (1, 0) | **2476.92** | 2476.9 | 2497 |
| 6 | (0, 0) | **35.6347** | 35.62 | 35.73 | 25 | (1, 1) | **2684.44** | 2684.4 | 2713 |
| 7 | (0, 1) | **80.8957** | 80.895 | 80.8 | 26 | (1, 1) | **2870.64** | 2870.6 | 2945 |
| 8 | (1, 0) | **80.8957** | 80.895 | 80.8 | 27 | (0, 1) | **3004.55** | 3003.5 | 3240 |
| 9 | (0, 1) | **235.387** | 235.38 | 237.1 | 28 | (1, 0) | **3004.55** | 3003.5 | 3240 |
| 10 | (1, 0) | **235.387** | 235.38 | 237.1 | 30 | (0, 1) | **3774.07** | 3774.1 | 3927 |
| 11 | (0, 0) | **269.328** | 269.31 | 226.0 | 30 | (1, 0) | **3774.07** | 3774.1 | 3927 |
| 12 | (1, 1) | **320.685** | 320.67 | 316.1 | 31 | (0, 0) | **5114.01** | 5112.8 | 5480 |
| 13 | (1, 1) | **375.218** | 375.22 | 378 | 32 | (0, 0) | **5460.70** | 5459.9 | 5640 |
| 14 | (0, 1) | **730.123** | 730.12 | 746 | 33 | (1, 1) | **5503.14** | 5503.1 | 5570 |
| 15 | (1, 0) | **730.123** | 730.12 | 746 | 34 | (0, 0) | **5619.53** | 5619.1 | 5640 |
| 16 | (0, 0) | **876.237** | 876.42 | 886 | 35 | (1, 1) | **5698.55** | 5698.5 | 6303 |
| 17 | (0, 0) | **933.829** | 933.84 | 941 | 36 | (0, 1) | **5959.69** | 5958.9 | 6036 |
| 18 | (0, 1) | **1103.37** | 1103.38 | 1131 | 37 | (1, 0) | **5959.69** | 5958.9 | 6036 |
| 19 | (1, 0) | **1103.37** | 1103.38 | 1131 | 38 | (0, 0) | **7236.24** | 7235.8 | 7310 |
| 20 | (1, 1) | **1525.91** | 1525.88 | 1554 | 39 | (0, 0) | **7505.22** | – | 7840 |
| 21 | (0, 0) | **1700.85** | 1700.91 | 1702 | 40 | (0, 1) | **8527.41** | – | 9030 |
| 22 | (0, 0) | **1813.12** | 1812.68 | 2020 | 41 | (1, 0) | **8527.41** | – | 9030 |

**Table 4**
Dimensionless nonzero frequency parameters for completely free plates with three different aspect ratios using the present method compared with Gorman [65], Ritz [29,64,15] methods as well as WEM method [61].

| $b/a$ | Method | 4 | 5 | 6 | 7 | 8 | 9 | 10 | 11 |
|---|---|---|---|---|---|---|---|---|---|
| $\nu = 0.333, \lambda = \omega a^2\sqrt{\rho h/D}$ | | | | | | | | | |
| 0.5 | | (0, 0) | (1, 1) | (0, 1) | (1, 0) | (0, 0) | (1, 1) | (1, 0) | (0, 0) |
| | **S-DSM** | **5.31026** | **6.49344** | **14.3372** | **14.7682** | **21.9052** | **24.9782** | **25.8108** | **29.5260** |
| 1 | | (1, 1) | (0, 0) | (0, 0) | (0, 1) | (1, 0) | (0, 1) | (1, 0) | (0, 0) |
| | **S-DSM** | **3.29214** | **4.80596** | **6.10571** | **8.55815** | **8.55815** | **15.2330** | **15.2330** | **15.6893** |
| | GSM [65] | 3.292 | 4.806 | 6.106 | 8.558 | 8.558 | 15.23 | 15.23 | 15.69 |
| 2 | | (0, 0) | (1, 1) | (1, 0) | (0, 1) | (0, 0) | (1, 1) | (0, 1) | (0, 0) |
| | **S-DSM** | **1.32756** | **1.62336** | **3.58430** | **3.69205** | **5.47631** | **6.24454** | **6.45271** | **7.38149** |
| | GSM [65] | 1.328 | 1.623 | 3.584 | 3.692 | 5.476 | 6.245 | 6.453 | 7.381 |
| $\nu = 0.3, \lambda = 4\omega a^2\sqrt{\rho h/D}$ | | | | | | | | | |
| 0.5 | | (0, 0) | (1, 1) | (0, 1) | (1, 0) | (0, 0) | (1, 1) | (1, 0) | (0, 0) |
| | **S-DSM** | **21.4631** | **26.5749** | **58.4820** | **59.6061** | **88.0097** | **101.503** | **104.002** | **118.726** |
| | Ritz (poly.) [64] | 21.463 | 26.575 | 58.483 | 59.620 | 88.080 | 101.53 | 104.02 | – |
| 1 | | (1, 1) | (0, 0) | (0, 0) | (0, 1) | (1, 0) | (0, 1) | (1, 0) | (0, 0) |
| | **S-DSM** | **13.4682** | **19.5961** | **24.2702** | **34.8009** | **34.8009** | **61.0932** | **61.0932** | **63.6861** |
| | Ritz (t-p) [29] | 13.468 | 19.596 | 24.270 | 34.801 | 34.801 | 61.093 | – | – |
| | Ritz (poly.) [64] | 13.468 | 19.596 | 24.271 | 34.801 | 34.801 | 61.111 | 61.111 | – |
| | Ritz (beam) [15] | 13.489 | 19.789 | 24.432 | 35.024 | 35.024 | 61.526 | 61.526 | – |
| | WEM [61] | 13.47 | 19.61 | 24.28 | 34.82 | 34.82 | 61.13 | 61.13 | 63.72 |
| 2 | **S-DSM** | **5.36579** | **6.64373** | **14.6205** | **14.9015** | **22.0024** | **25.3757** | **26.0005** | **29.6814** |

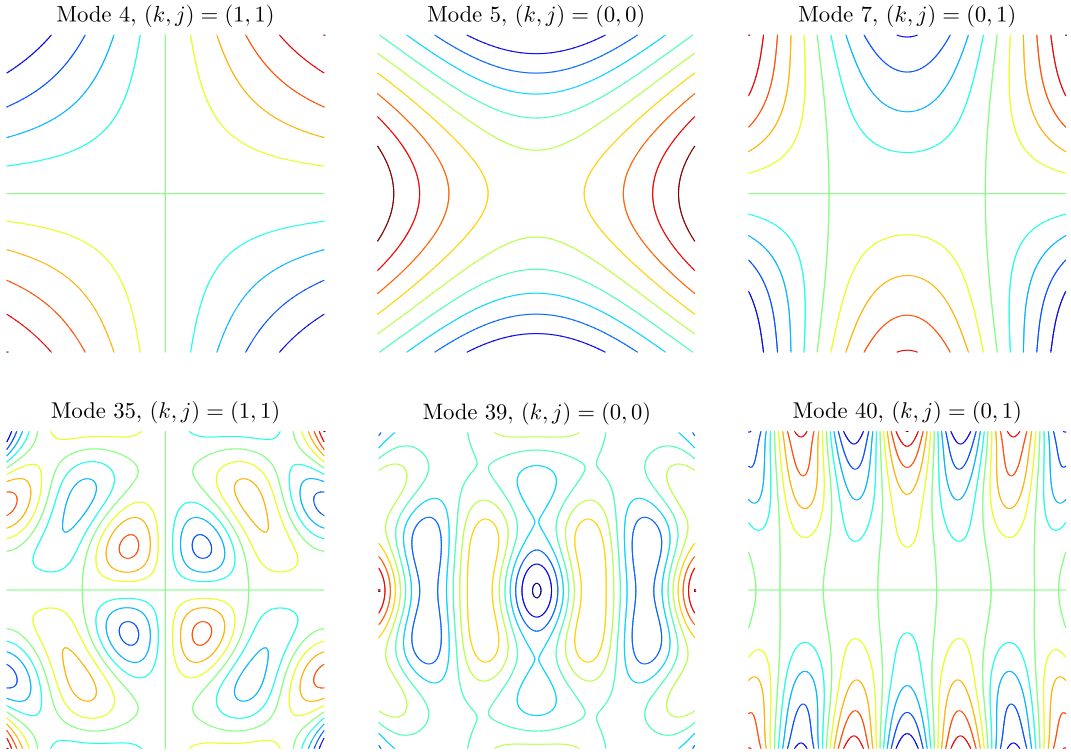


**Fig. 2.** Representative mode shapes with different $(k,j)$ symmetric/antisymmetric properties of an FFFF isotropic square plate, namely, the 4, 5, 7, 35, 39 and 40th modes.

not a complete set. This is surely a mistake made by Rosales and Filipich [66]. As a matter of fact, the second dimensionless frequency parameter $\omega a^2\sqrt{\rho h/D}$ with $\nu = 0.3$ in Table 4 of Ref. [65] by Gorman is 4.899 (plate dimension $a \times a$), which can be easily transformed into 19.60 in terms of the dimensionless parameter $\omega(2a)^2\sqrt{\rho h/D}$ (plate dimension $2a \times 2a$).

Also, one can make another observation from Table 4 that the results of both the Ritz methods as well as the variation-based WEM serve as the upper bounds for the S-DSM solutions, as expected.

*5.3.2. Fully clamped case*

A rectangular plate with fully clamped edges is a very common case in many engineering structures, whose free vibration analysis has received wide attention and extensive coverage in the literature. In Table 5 the first eight natural frequencies are obtained by the S-DSM for three plate aspect ratios ($b/a = 0.5,\ 1$ and 2). These are compared with results obtained from thirteen other typical methods. The number of terms used in the basis functions for different methods and the number of significant digits of the computed results are also included in the last two columns of the

**Table 5**
Dimensionless frequency parameter for fully clamped rectangular plates with three aspect ratios. Results computed by the present method are compared with those obtained using other methods.

| $b/a$ | Method | $\lambda = 4\omega a^2\sqrt{\rho h/D}$ | | | | | | | | $M = N$ | Signif. digits |
|---|---|---|---|---|---|---|---|---|---|---|---|
| | | 1 | 2 | 3 | 4 | 5 | 6 | 7 | 8 | | |
| 0.5 | | (1, 1) | (2, 1) | (3, 1) | (4, 1) | (1, 2) | (2, 2) | (3, 2) | (5, 1) | | |
| | **S-DSM** | **98.31084** | **127.3039** | **179.0786** | **253.3230** | **255.9325** | **284.3050** | **333.0908** | **349.0107** | **5/11/16** | **5/6/7** |
| | FSA[a] | 98.309 | 127.30 | 179.07 | 253.31 | 255.92 | 284.29 | – | – | 17 | 4 |
| | NSV[b] | 97.542 | 125.751 | 177.613 | – | 255.678 | 283.509 | 331.85 | – | 1 | 2 |
| | Ext. Kant.[c] | 98.324 | 127.333 | 179.115 | – | 255.939 | 284.325 | 333.125 | – | – | 4 |
| 1 | | (1, 1) | (1, 2) | (2, 1) | (2, 2) | (1/3–3/1) | (1/3 + 3/1) | (2, 3) | (3, 2) | | |
| | **S-DSM** | **35.98519** | **73.39385** | **73.39385** | **108.2165** | **131.5808** | **132.2048** | **165.0004** | **165.0004** | **5/11/16** | **5/6/7** |
| | FSA[a] | 35.985 | 73.393 | 73.393 | 108.21 | 131.58 | 132.20 | – | – | 17 | 5 |
| | NSV[b] | 35.112 | 72.899 | 72.899 | 107.47 | 131.63* | 131.63* | 164.39 | 164.39 | 1 | 2 |
| | UISSM[d] | 35.9852 | 73.3938 | ★★ | 108.2165 | 131.5808 | 132.2048 | – | – | – | 6 |
| | IM (DTS)[e] | 35.98519 | 73.39385 | 73.39385 | 108.2165 | 131.5808 | 132.2048 | – | – | 360 | 7 |
| | GDQ[f] | 35.985 | 73.394 | 73.394 | 108.21 | 131.58 | 132.20 | 165.00 | 165.00 | 24 | 5 |
| | DSC(LK)[g] | 35.989 | 73.407 | 73.407 | 108.25 | 131.62 | 132.24 | 165.07 | 165.07 | 24 | 4 |
| | Ritz (*pb*-2)[h] | 35.985 | 73.394 | 73.394 | 108.22 | 131.58 | 132.20 | 165.00 | 165.00 | 16 | 5 |
| | Ritz (plate)[i] | 35.985 | 73.394 | 73.394 | 108.22 | 131.58 | 132.21 | 165.00 | 165.00 | 30 | 5 |
| | Ritz (trig.)[j] | 35.986 | 73.395 | 73.395 | 108.22 | 131.59 | 132.21 | 165.01 | 165.01 | 50 | 4 |
| | Ritz (beam)[k] | 35.992 | 73.413 | 73.413 | 108.27 | 131.64 | 132.24 | – | – | 6 | 3 |
| | Ritz (poly.)[l] | 35.985 | 73.395 | 73.395 | 108.22 | 131.78 | 132.41 | – | – | 6 | 3 |
| | Ritz (t-p)[m] | 35.986 | 73.397 | 73.397 | 108.225 | 131.592 | 132.215 | – | – | 40 | 4 |
| | Ext. Kant.[c] | 35.999 | 73.405 | 73.405 | 108.24 | 131.90* | 131.90* | 165.02 | 165.02 | – | 3 |
| 2 | | (1, 1) | (1, 2) | (1, 3) | (1, 4) | (2, 1) | (2, 2) | (2, 3) | (1, 5) | | |
| | **S-DSM** | **24.57771** | **31.82597** | **44.76966** | **63.33075** | **63.98313** | **71.07625** | **83.27270** | **87.25267** | **5/11/16** | **5/6/7** |
| | UISSM[d] | 24.5777 | 31.8260 | 44.7696 | ★★ | ★★ | 71.0763 | ★★ | 87.2526 | – | 6 |
| | IM (DTS)[e] | 24.57771 | 31.82598 | 44.76966 | 63.33076 | 63.98313 | – | – | – | 360 | 7 |
| | NSV[a] | 24.358 | 31.438 | – | – | 63.920 | 70.877 | – | – | 1 | 2 |
| | Ext. Kant.[c] | 24.581 | 31.833 | 44.779 | 63.340 | 63.985 | 71.081 | 83.281 | – | – | 3 |

[a] Fourier Series based Analytical method [11].
[b] Novel Separation of Variables [40].
[c] Extended Kantorovich [31–33].
[d] Untruncated Infinite Series Superposition Method [9].
[e] Iterative Method (Dual Trigonometric Series) [38].
[f] Generalised Differential Quadrature [67].
[g] Discrete Singular Convolution (Lagrange's delta kernel) [67].
[h] Ritz (*pb*-2 polynomials) [22].
[i] Ritz (plate characteristic functions) [68].
[j] Ritz (trigonometric functions) [24].
[k] Ritz (beam eigenfunctions) [15].
[l] Ritz (orthogonal polynomials) [16].
[m] Ritz (trigonometric functions and polynomials) [29].

table wherever available. Numerical simulations suggest that all of the S-DSM results converge to the 5th (6th or 7th) digit with $M = N \geqslant 5$ (11 or 16), which seems to be the fastest convergence rate compared with all other competing methods. Five amongst the thirteen methods are classified into the strong-form based methods, namely, the current S-DSM, Fourier series analytical method (FSA) [11], the novel separation of variable method (NSV) [40], untruncated infinite series superposition method (UISSM) [9] and iterative method based on dual trigonometric series (IM (DTS)) [38]. Evidently, all of the Ritz methods [15,16,22,24,29,68] using different basis functions and the extended Kantorovich method [31–33] belong to weak-form based methods.

In Table 5, the results from the current S-DSM match closely with those by UISSM [9] and IM(DTS) [38] which are presumably the most accurate results amongst all of the thirteen methods other than the S-DSM. This high level of accuracy is expected since these three methods are based on strong formulation and use complete set of series. The results from these three methods provide over six digit precision. However, the method IM(DTS) uses a very large number of dual trigonometric series ($360 \times 360$) and the UISSM [9] misses some of the natural frequencies (denoted by ★★ in Table 5). By using a $17 \times 17$ Fourier cosine series, FSA [11] leads to results with four to five digit accuracy. By using a $24 \times 24$ grid together with 23 ghost points extended from each edge, the GQD [67] gives five digit accuracy results whereas DSC [67] gives results up to four digit accuracy with a grid size $24 \times 24$.

The Ritz methods in Table 5 are based on six different basis functions [15,16,22,24,29,68]. It can be found that all of the results based on Ritz method serve as the upper bound as expected. The results in Ref. [22] using *pb*-2 polynomials and Ref. [68] using plate characteristic equations are of better accuracy than the others [15,16,24,29]. Even though the trigonometric basis function adopted in Ref. [24] was proven to be applicable to higher order modes [23], the convergence rate is not so fast: a series with 50 terms give only four digit accuracy. The set of trigonometric functions and polynomials used in Ref. [29] give accurate results for the completely free case (see Table 4) but its convergence rate is comparatively slower for the fully clamped case: a 40-term series only leads to four digit accuracy results. This might be due to the involvement of the penalty method in Ref. [29]. The extended Kantorovich methods [31–33] also lead to upper bound results with three digit accuracy. Inaccuracy always occurs when this type of methods are applied to non-Levy-type plates no matter whether the reduction is following either an iterative procedure [31,32] or an analytical procedure [33]. This is due to the nature of this method which will be further examined in Section 6.

Another interesting point which is worth mentioning is the so-called 'degenerate mode' for a square isotropic plate. For notational convenience, a mode with $\hat{m}$ and $\hat{n}$ half-waves in $x$ and $y$ directions

respectively is denoted as the $(\hat{m}, \hat{n})$ mode. If the nodal lines are assumed to be parallel to the $x$ and $y$ axes, there will be $(\hat{m}-1)$ and $(\hat{n}-1)$ nodal lines parallel to $y$ and $x$ coordinates respectively. However, this assumption is generally not valid for non-Levy plates. In Table 5, the notations (1/3 – 3/1) or (1/3 + 3/1) represent the first two so-called 'degenerate modes' with non-parallel nodal lines when considering the clamped isotropic square plates. The first four degenerate modes are shown in Fig. 3. It is clear that the nodal lines of the 5th (1/3 – 3/1) and the 16th (1/5 – 5/1) modes are essentially the diagonal lines of the rectangular plate whereas the nodal lines of the 6th (1/3 + 3/1) and the 17th (1/5 + 5/1) modes are not straight at all. These degenerate modes can neither be predicted by the extended Kantorovich method [31–33] nor by the separation of variable method given by Xing and Liu [40] (see the values with superscript '$*$' in Table 5), but can be captured by other methods including the current S-DSM. This is because of the problematic series used in the Kantorovich and the separation of variable methods. The details will be explained later in Section 6.

### 5.4. Three other practical cases

The free vibration of a rectangular plate with different classical boundary conditions have been covered by many investigations such as Leissa's classical monograph [69]. Nevertheless, there are relatively few accurate results reported in the literature. In this section, we revisit three cases with particular practical importance in engineering by using the present S-DSM in order to provide exact solutions. The three cases are: a cantilever plate (CFFF), a hinged plate (SFFF) and a plate with three edges clamped and the fourth edge free. All of the S-DSM results presented in this section are accurate up to six digit precision so that they can be used for benchmark purposes.

The cantilever plate problem is of common practical interest. In particular, an aircraft wing in aeronautical engineering can be ideally modelled as a cantilevered plate in the first instance. This problem has been studied extensively both numerically and experimentally. The first eight natural frequencies with six digit accuracy are shown in Table 6, where 'S' and 'A' stand for the symmetric and antisymmetric natural modes. In the first part of Table 6, the S-DSM results with $\nu = 0.3$ are compared with those by four types of Ritz methods [15,22,24,29] as well as by the Fourier series based analytical method [11]. In the second part of Table 6, the S-DSM results with $\nu = 0.333$ are compared with the Gorman's superposition method [70]. The Ritz methods (weak-form based) in Refs. [15,22,24,29] give the upper-bound solutions while the boundedness of the Fourier series based analytical method [11] (strong-form based) is apparently case dependent. The results by Gorman's superposition method [70] provide accurate results up to four digit accuracy, all of which coincide with the first four digit of the results from the present method. The first four mode shapes of a CFFF plate with $b/a = 0.5, \nu = 0.3$ are illustrated in Fig. 4. The first and third modes are symmetric whilst the second and fourth ones are antisymmetric.

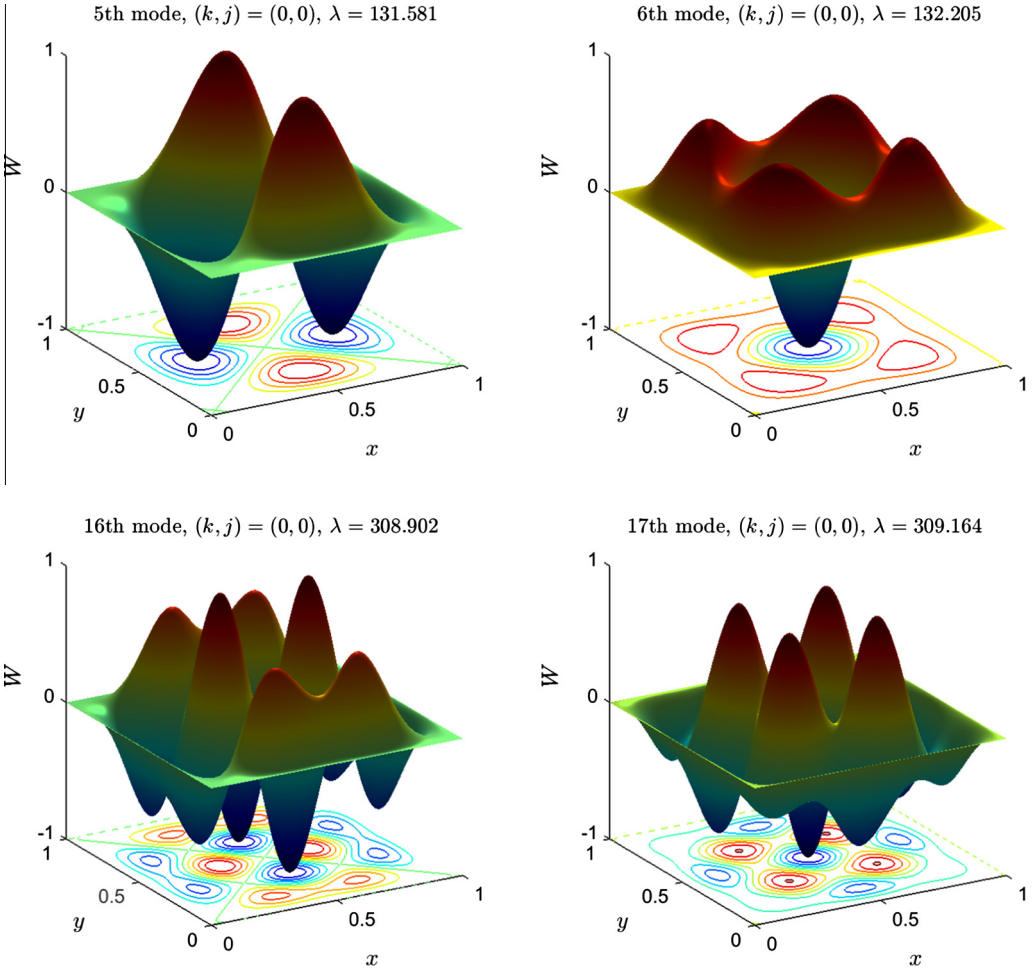


**Fig. 3.** The first four degenerate mode shapes for a clamped square isotropic plate ($\nu = 0.3$), namely, the 5th (1/3 – 3/1), 6th (1/3 + 3/1), 16th (1/5 – 5/1) and the 17th (1/5 + 5/1) modes.

**Table 6**
Dimensionless natural frequencies for a CFFF plate computed by the current S-DSM for different plate aspect ratios and different Poisson's ratios. Side by side are the results by Fourier series based analytical method [11], four Ritz methods using different admissible functions [15,22,24,29] and Gorman's superposition method [70].

| $b/a$ | Method | $\lambda = 4\omega a^2\sqrt{\rho h/D}$ | | | | | | | |
|---|---|---|---|---|---|---|---|---|---|
| | | 1 | 2 | 3 | 4 | 5 | 6 | 7 | 8 |
| $\nu = 0.3$ | | | | | | | | | |
| 0.5 | | S | A | S | A | S | A | S | S |
| | **S-DSM** | **3.43923** | **14.8013** | **21.4331** | **48.1758** | **60.1478** | **92.5154** | **93.1014** | **118.447** |
| | FSA [11] | 3.439 | 14.800 | 21.430 | 48.171 | 60.143 | 92.507 | – | – |
| 1 | | S | A | S | S | A | S | S | A |
| | **S-DSM** | **3.47100** | **8.50619** | **21.2839** | **27.1987** | **30.9542** | **54.1836** | **61.2534** | **64.1420** |
| | FSA [11] | 3.470 | 8.504 | 21.279 | 27.201 | 30.948 | 54.185 | – | – |
| | Ritz (t-p) [29] | 3.471 | 8.507 | 21.285 | 27.199 | 30.957 | 54.188 | – | – |
| | Ritz (trig.) [24] | 3.4711 | 8.5066 | 21.285 | 27.199 | 30.956 | 54.187 | 61.255 | 64.142 |
| | Ritz (*pb*-2) [22] | 3.4714 | 8.5083 | 21.288 | 27.199 | 30.962 | 54.195 | 61.260 | 64.163 |
| | Ritz (beam) [15] | 3.4917 | 8.5246 | 21.429 | 27.331 | 31.111 | 54.443 | – | – |
| 2 | | S | A | S | S | A | S | S | A |
| | **S-DSM** | **3.49279** | **5.35093** | **10.1805** | **19.0747** | **21.8379** | **24.6698** | **31.4252** | **34.0283** |
| $\nu = 0.333$ | | | | | | | | | |
| 1 | | S | A | S | S | A | S | S | A |
| | S-DSM | **3.45955** | **8.35603** | **21.0887** | **27.0645** | **30.5510** | **53.5228** | **61.1157** | **63.6162** |
| | GSM [70] | 3.459 | 8.356 | 21.09 | 27.06 | 30.55 | 53.53 | 61.12 | 63.62 |
| 2 | | S | A | S | S | A | S | S | A |
| | S-DSM | **3.48693** | **5.27817** | **10.0323** | **18.8402** | **21.7831** | **24.5540** | **31.0664** | **33.8824** |
| | GSM [70] | 3.487 | 5.278 | 10.03 | 18.84 | 21.78 | 24.55 | 31.07 | 33.88 |

Table 7 shows natural frequencies for the other two cases, i.e., SFFF and CCCF. A SFFF rectangular plate is a model for hinged gates encountered frequently, for example, in the field of civil, aeronautical and hydraulic engineering. However, this case has only received sporadic attention [15]. It should be emphasised that the first mode for a SFFF plate is rigid body rotation mode corresponding to zero natural frequency, which can be captured by the current S-DSM due to the application of the WW algorithm. Table 7 includes only nonzero natural frequencies of an SFFF plate starting from the second mode. Meanwhile, a plate with three clamped and one free edges is another case with much practical importance. The results by the current S-DSM are compared with those by three Ritz methods [15,19,29] and the extended Kantorovich method [32]. In both SFFF and CCCF cases, the results obtained by the Ritz methods in Refs. [15,19] and the extended Kantorovich method [32] in Table 7 only have two digit precision, and the results from Ref. [29] have four digit precision, which are compared to the present S-DSM results having six figure accuracy.

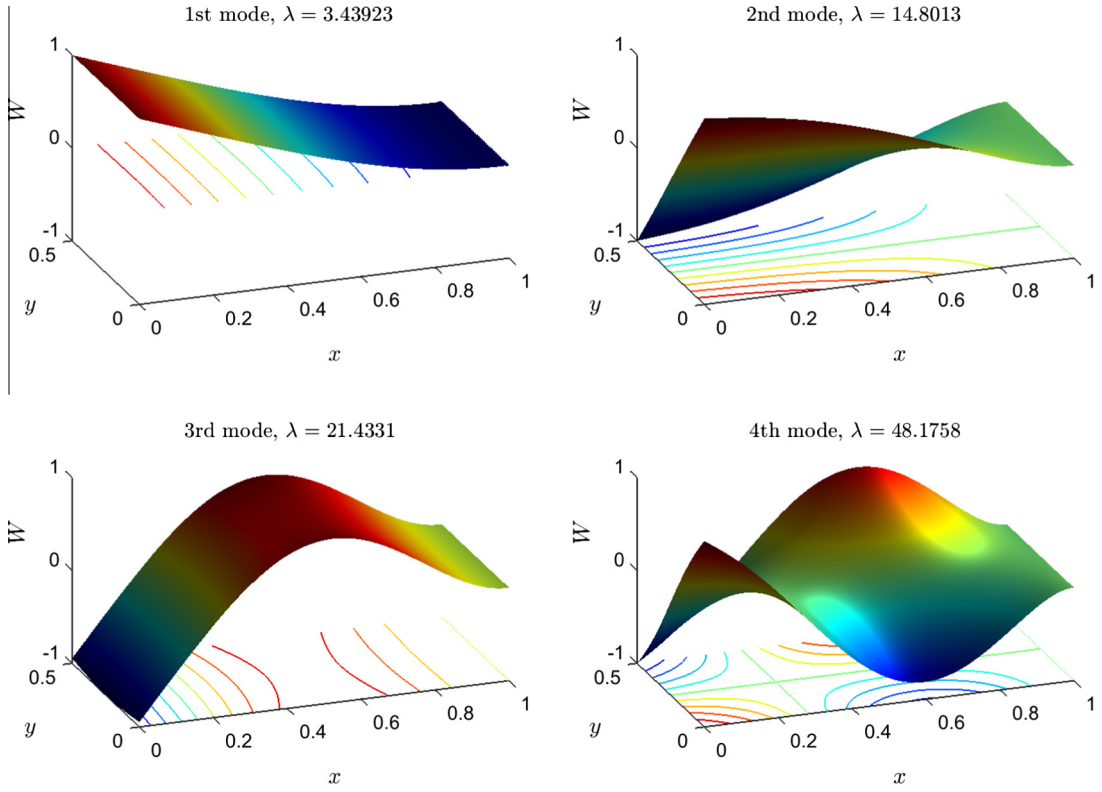


**Fig. 4.** The first four mode shapes of a cantilevered isotropic rectangular plate ($b/a = 0.5, \nu = 0.3$).

**Table 7**
Dimensionless nonzero natural frequencies for the SFFF and CCCF cases with different aspect ratios. The results of the current S-DSM are compared with those obtained by three Ritz methods [15,19,29] and extended Kantorovich method [32].

| $b/a$ | Method | $\lambda = 4\omega a^2\sqrt{\rho h/D}$ | | | | | | | |
|---|---|---|---|---|---|---|---|---|---|
| *SFFF* | | | | | | | | | |
| | | 2 | 3 | 4 | 5 | 6 | 7 | 8 | 9 |
| 0.5 | **S-DSM** | **13.0387** | **14.8448** | **42.8417** | **48.5443** | **82.9967** | **91.8028** | **103.169** | **122.651** |
| 1 | **S-DSM** | **6.64372** | **14.9015** | **25.3757** | **26.0005** | **48.4495** | **50.5785** | **58.7420** | **65.1796** |
| | Ritz (t-p) [29] | 6.644 | 14.902 | 25.376 | 26.001 | 48.450 | 50.579 | – | – |
| | Ritz (beam) [15] | 6.6480 | 15.023 | 25.492 | 26.126 | 48.711 | 50.849 | – | – |
| 2 | **S-DSM** | **3.36705** | **8.70022** | **15.2733** | **17.3163** | **19.2929** | **26.3651** | **32.8673** | **38.2112** |
| *CCCF* | | | | | | | | | |
| | | 1 | | 3 | 4 | 5 | 6 | 7 | 8 |
| 0.5 | **S-DSM** | **31.1010** | **70.1452** | **103.398** | **128.860** | **144.088** | **204.755** | **207.237** | **259.661** |
| | Ext. Kant. [32] | 31.703 | 70.520 | 104.234 | 129.023 | 144.964 | 205.222 | 205.222 | 259.867 |
| 1 | **S-DSM** | **23.9184** | **39.9953** | **63.2159** | **76.7082** | **80.5661** | **116.650** | **122.225** | **134.427** |
| | Ext. Kant. [32] | 24.013 | 40.200 | 63.319 | 76.890 | 80.698 | 116.84 | 122.32 | – |
| | Ritz (t-p) [29] | 23.921 | 39.999 | 63.224 | 76.713 | 80.576 | 116.665 | – | – |
| | Ritz (*pb*-2) [19] | 23.97 | 40.12 | 63.43 | 76.72 | – | – | – | – |
| | Ritz (beam) [15] | 24.020 | 40.039 | 63.493 | 76.761 | 80.713 | 116.80 | – | – |
| 2 | **S-DSM** | **22.6318** | **26.0188** | **33.7543** | **46.7023** | **61.8658** | **65.0787** | **65.9093** | **74.1859** |
| | Ext. Kant. [32] | 22.672 | 26.057 | 33.806 | – | 61.915 | – | 65.947 | 74.227 |

It should be noted that all of the weak-form based solutions in Refs. [15,19,32,29] serve as the upper bound solutions as expected.

## 6. Discussions of and insight into different analytical methods for free vibration of rectangular plates

The comparison of the current S-DSM with a wide range of existing methods in the last section enables the discussion of different methods for free vibration analysis of rectangular plates. In Section 6.1, different series-based solutions are classified into three types and the completeness of series solution is discussed. Then an explanation is given in Section 6.2 for why closed-form solution is available only for Levy-type plates. Finally, Section 6.3 gives specific as well as general conclusions on the suitability or otherwise of various analytical methods for the free vibration of rectangular plates.

### 6.1. Three types of series solutions and discussion on the completeness

In the literature, possible exact solutions for non-Levy type solutions are generally available only in series form, but different series solutions have different attributes regarding the convergence and accuracy of the solution. Irrespective of whether the method is strong- or weak-form based, there are mainly three types of solutions for free vibration analysis of rectangular plates.

#### 6.1.1. The first type of solutions

The first type of solutions have the following series form

$$W(x,y) = X(x)Y(y) = \sum_{m,n=1}^{\infty} C_{mn}X_m(x)Y_n(y). \tag{46}$$

In Eq. (46), both of the basis functions $X_m(x)$ and $Y_n(y)$ should form a complete set for the 1D functions $X(x)$ and $Y(y)$ within the corresponding intervals. The series solution of Eq. (46) therefore form a complete series expansion in the defined domain, according to the statement on page 56 of Ref. [71]. The coefficients $C_{mn}$ are determined by the GDE and/or the BC. The above type of series is identical if the $x$ and $y$ are interchanged in the expressions. Alternatively, it can be said that the expressions of the series of Eq. (46) are *symmetric* in terms of the variables $x$ and $y$. This also includes four subtypes.

(i) Both $X_m(x)$ and $Y_n(y)$ are obtained by solving 1D functions $X(x)$ and $Y(y)$ with the corresponding BC of an appropriate equivalent beam. The unknown coefficients $C_{mn}$ are determined from the GDE and BC either in strong or weak form. For example, Ritz [3] ingeniously made the assumption that the eigenmodes of a completely free plate is described in the form of Eq. (46), where $X_m(x)$ and $Y_n(y)$ are the characteristic functions of the corresponding elastic beams with free edges. Similar idea was used later by Warburton [14], Leissa [15] and Ding [72] covering plates with various BC.

(ii) There are also orthogonal series satisfying all the geometric BC of the plate [16,19,23], whose coefficients are determined by satisfying the GDE. For example, Bhat [16] proposed a set of orthogonal polynomials obtained from Gram-Schmidt process, which is modified by Liew et al. into *pb*-2 polynomials and applied to various plate problems [19–22]. Beslin and Nicolas [23] proposed a hierarchical trigonometric set applicable to medium frequency range which was then used by Dozio [24] when applying Ritz method.

(iii) Sakata and Hosokawa [38] used double trigonometric series. The series satisfies the GDE and part of the BC, and the rest of the BC are then transferred into an infinite set of simultaneous equations.

(iv) Li et al. [11] used a complete 2D Fourier cosine series supplemented with several 1D Fourier series which can be applied to plates with various BC. Satisfying first the BC and then the GDE in strong form leads to the final eigenvalue problem. Monterrubio and Ilanko [29] used a complete set which is combined by trigonometric functions and polynomials, and the constraints were modelled by using the penalty method.

However, all of the above methods based on Eq. (46) are not very computationally efficient. If $m \in [1, M]$ and $n \in [1, N]$ are taken, there will be $M \times N$ number of $C_{mn}$ involved in the computation. Besides, subtypes (i) and (ii) above are essentially suitable for plates with uniformly prescribed BC on each edge and subtype (iii) was only applied to fully clamped case. In terms of numerical stability, almost all of the solutions of subtype (i) [14,15,72] and some of subtype (ii) [16,19–22] generally experience numerical singularity when evaluated at higher orders. The subtype (iv) solutions may also lead to numerical singularity either arising from modelling general BC as elastic constraints [11] or from the artificial penalty values which may introduce round-off errors [29]. The singularity might become more severe under certain specific BC.

This may prevent these method from computing highly accurate results, particularly within higher frequency range. To sum up, the above four subtypes of series solutions appear to have no specific mathematical significance with respect to the convergence and accuracy of their results.

#### 6.1.2. The second type of solutions

The second type of solutions take the form:

$$W(x,y) = X^*(x)\widehat{Y}(y), \tag{47}$$

where the solution component $X^*(x)$ is the pre-assumed solution in the $x$ direction whereas $\widehat{Y}(y)$ is deduced analytically from the GDE based on $X^*(x)$. (Of course, Eq. (47) is also a representative of $W(x,y) = Y^*(y)\widehat{X}(x)$ by just interchanging the variables $x$ and $y$.) Notice that the type of solutions described in Eq. (47) also include the solutions in which the $X^*(x)$ is expressed in terms of a complete series (spectral method). In this case, $X^*(x) = \sum_m^\infty C_m X_m^*(x)$ and thus $W(x,y) = \sum_m^\infty C_m X_m^*(x)\widehat{Y}_m(y)$, where $\widehat{Y}_m(y)$ are derived analytically from the GDE based on $X_m^*(x)$.

However, the type of solutions based on Eq. (47) are incapable of giving exact solution with the only exception for Levy-type plates. This is because this type of solutions are based on a problematic assumption that the solution component in only one direction is chosen *a priori* [6,32]. This is obviously not a 'fully physical' assumption for the general case. Actually, the solution components in both $x$ and $y$ directions should be obtained simultaneously when solving the original eigen-boundary value problem. To look at it from another aspect, the assumption of Eq. (47) is equivalent to enforcing the nodal lines of the mode shapes of rectangular plates to be parallel to the plate edges, which is not a 'physical' assumption for the general case. The type of solutions of Eq. (47) have been used in the Kantorovich method [6] and its derivatives like the extended Kantorovich method [31–33] which only led to approximate solutions due to the aforementioned reasons. For example, Eq. (7) in Ref. [32] is obviously an approximate assumption by taking $\delta W = X\delta Y + Y\delta X = Y\delta X$, and that is why it only gave approximate results. Consequently, as can be seen from Tables 5 and 7 (non-Levy type cases), all of the results by Kantorovich-type methods [31–33] are not sufficiently accurate which cannot be further improved, no matter whether the reduction procedure is realised iteratively [31,32] or analytically [33]. Also, as pointed out in Refs. [38,32], the Kantorovich-type methods are incapable of predicting mode shapes for plates whose nodal lines are not parallel to the $x$ and $y$ axes. Notice that this statement does not necessarily imply that the methods based on the assumption of Eq. (47) will always give accurate solution for the natural modes whose nodal lines are parallel to both axes. The appearance of nodal lines parallel to axes can also occur because of the symmetry of the boundary conditions for non-Levy cases (e.g., for fully clamped or completely free plates), whose natural frequencies cannot be predicted accurately by the method based on Eq. (47). It should be noted that the expression of Eq. (47) does not remain identical when interchanging the variables $x$ and $y$: the expression of Eq. (47) is not *symmetric* in terms of the variables $x$ and $y$.

#### 6.1.3. The third type of solutions

The third type of solutions can be seen as a combination of two sets of the second type of solutions in Eq. (47), namely,

$$W(x,y) = \sum_{m=1}^{\infty} X_m^*(x)\widehat{Y}_m(y) + \sum_{n=1}^{\infty} Y_n^*(y)\widehat{X}_n(x). \tag{48}$$

In Eq. (48), the series $X_m^*(x)$ and $Y_n^*(y)$ are complete sets for 1D functions with arbitrary boundary conditions, whereas $\widehat{Y}_m(y)$ and $\widehat{X}_n(x)$ are determined analytically based on the GDE. Obviously, each component $X_m^*(x)\widehat{Y}_m(y)$ or $Y_n^*(y)\widehat{X}_n(x)$ and thus their sum in the form of Eq. (48) satisfy the GDE exactly. Moreover, it can be proved mathematically that the series solution of Eq. (48) form a complete set for the solution space of the GDE (within the defined region) with all of the BC remaining unspecified. Also, the evaluation of such a series solution on the boundaries form a complete set for any arbitrary BC. Apparently, this type of series solution of Eq. (48) is physically more reasonable. It is understandable that the solutions based on Eq. (48) have the superiority to approach the exact solutions over the previous two types of solutions. Besides, this type of series is very computationally economic. When $m \in [1, M]$ and $n \in [1, N]$ for a GDE with the highest derivative order (*HDE*), only $HDE \times (M + N)$ unknowns are involved. This is a much smaller number compared with that of Eq. (46). It is clear from the formulation in Sections 2 and 3 that the current S-DSM belongs to the third type. It is worth pointing out that Gorman's superposition method [7,8] (GSM) is quite similar with the series solution used in the current S-DSM. The difference is that the series solution of GSM is a representation of the solution space corresponding to the GDE with specific BC whereas that of the S-DSM is a representation of the solution space of GDE with BC unspecified. Therefore, the solution space of GSM can be regarded as a subspace of that of the current S-DSM.

#### 6.1.4. Completeness of series solutions

Apart from the above three types of series, there have been some other discussions in the literature [11,66,73] on the completeness of the series solutions for free vibration of plates. Hurlebaus et al. [73] used a Fourier cosine series solution whose completeness is questioned by Rosales and Filipich [66]. Rosales and Filipich [61,66] used a variation-based whole element method (WEM) based on a complete set of trigonometric functions in $L_2$. Although these series solutions were claimed to be capable of calculating the exact natural frequencies and mode shapes, it later appeared to be untrue and the problem was due to the very slow convergence rate. As pointed out by Li et al. [11], this is maybe because their series is smooth for only the first- and second-order derivative which prevented the method to compute the natural frequencies and mode shapes to any arbitrary accuracy. Referring to Gorman's superposition method [65] (GSM), the arguments by Rosales and Filipich [66] appear to be a misunderstanding as mentioned earlier in Section 5. In fact, the series function used in GSM [65] does form a complete set for the studied problems with specific boundary conditions. Consequently, it exhibits a much faster convergence rate than that of the WEM [66], as evident in Table 4.

Besides, sufficient number of terms to be used in the series solution is indeed a crucial factor. Here two examples are worth mentioning.

(i) Due to the non-existence of computers in 1909, Ritz [3] used only the *dominant* terms $X_m(x)Y_n(y) \pm X_n(x)Y_m(y)$ of the first type series in Eq. (46) and therefore, the results deteriorated for the modes higher than, say, the tenth one, see Table 3. This is because the role played by *non-dominant* terms becomes important for higher modes.

(ii) It is worth noting that the so-called novel separation of variable method (NSV) proposed by Xing and Liu [40] is not really an exact method for non-Levy plates as claimed by the authors. It can be seen from Table 5 that their solutions are smaller than the accurate results and have only two digit precision. Bahrami et al. [42] have given a clear explanation for why their method [40] is not exact. Here an interpretation from another angle is given. The solutions in Ref. [40] can be regarded as using only one but dominant term in the series of Eq. (48) which is not a complete series solution for

non-Levy type plates. Therefore, their results in Ref. [40] can be regarded as approximate solutions. This is at best similar to the current S-DSM with only one term in the series. It becomes evident by recalling the aforementioned boundedness analysis for the CCCC case in Section 5.1. For example, when $M = N = 2$ as in Table 1, the results of the current S-DSM are smaller than the converged results but more accurate than those of Ref. [40]. As $M(= N)$ increases, the results converge from below. Similar reasons apply to the symplectic elasticity method [43–45] which gives exact solutions only for Levy-type plates but not so for non-Levy-type plates.

To conclude, the results of the above two cases are not accurate due to the insufficiency of the series terms used.

### 6.2. Discussion on the closed-form exact solution

As mentioned earlier, the exact solution without resorting to series solution for free vibration of rectangular plates is only limited to Levy type plates with simple [4] and/or guided supports [5] on two opposite edges. (Navier solution is a special case when all edges of the plate are simply supported.) This has been universally acknowledged, but not sufficiently explained. This section aims to provide physical and mathematical insights into this issue.

It will be instructive to look at this problem from a wave propagation point of view (physically) in conjunction with spectral concept (mathematically). Physically, a natural mode shape of a structure is essentially a standing wave with the natural frequency propagating on the structure. It can be seen as a superposition of a series of waves with different wavenumbers travelling forward and backward with the same frequency. These waves reflect back when they reach the boundaries. Mathematically, the separation of variables used in Eq. (5) leads to the characteristic equation of Eq. (6), which defines the relationship amongst the wave parameters $q, p$ and the natural frequency $\omega$. Considering both the physical and mathematical aspects together will make physical meaning of the characteristic equation more clear: a wave with parameter $q$ and natural frequency $\omega$ travelling in the $x$ direction will lead to pairs of forward and backward waves with parameters $p$ in the $y$ direction which are the roots of the characteristic equation of Eq. (6) and vice versa.

For Levy-type plates, when transverse waves are propagating between a pair of simple or guided constraints, they will reflect back in such a way that all harmonic waves in this direction can be decoupled into sine or cosine waves. As a results, the deformation amplitude in the corresponding direction can be exactly represented by sinusoidal functions and the deformation amplitude in the other direction can be derived analytically. This is the only case in which the solution component in one direction can be assumed *a priori* and the solutions in the form of Eq. (47) can lead to closed-form exact solutions. Also, the nodal lines of the mode shape of Levy-type plates are always parallel to the axes. For non-Levy-type plates, the solution components in $x$ or $y$ direction cannot be assumed *a priori* alone and should be calculated simultaneously. Furthermore, as discussed in the previous section, the solution should be general enough to form a complete solution space of the GDE with the corresponding BC. Therefore, one can come to the conclusion that the Levy-type cases are the only special cases where the solution component in one direction $X(x)$ can be assumed *a priori* (e.g., see Eq. (47)) which allows exact solutions. The exact solutions for non-Levy type cases are only available in series form.

### 6.3. Conclusions on analytical methods for free vibration of rectangular plates

Based on the above discussion, the following observations can be made on the analytical methods for free vibration analysis of plates regardless of the fact whether the method is based on strong- or weak-form.

(i) The exact solutions for non-Levy plate are available only in series form constituting a complete set for the complete solution space of the GDE.
(ii) The expression of the series should be identical if the variables $x$ and $y$ are interchanged in the expression, i.e., the series expression should be *symmetric* with respect to the variables $x$ and $y$.
(iii) The convergence rate of the series solution depends on how the GDE and BC are satisfied. More precisely, the better the series solution satisfies the GDE and all BC (both geometric and natural BC), the higher convergence rate it will behave. Also, smoothness with respect to the highest derivative in the GDE should be guaranteed.
(iv) The numerical stability is indeed another important issue when the series is evaluated at higher orders. This is closely related to the orthogonal properties of the chosen series. The numerical stability is usually the main obstacle for most of the other analytical methods pursuing exact results in the literature, because the orthogonality of the series terms may becomes weaker for higher orders and therefore leads to ill-conditioning matrices. Also, the involvement of penalty method may also lead to ill-conditioning matrices.
(v) With truncated series function, the weak-form methods normally give upper bound solution for the natural frequencies, while the boundedness of strong-form methods is case dependent.

The current S-DSM belongs to strong-form method and satisfies the above (i)–(iv) points. Consequently, its results converge to exact results with a very fast convergence rate. The numerical stability for any high order series in the current S-DSM is guaranteed by the strong orthogonality of the modified Fourier series on the boundaries. This is evident from the diagonal structure of the coefficient matrices as shown by Eq. (C.1) in Appendix C. Moreover, the application of the enhanced WW algorithm serves as an efficient and highly reliable solution technique for the ensuing transcendental eigenvalue problem. Consequently, any required natural frequencies can be computed within any desired accuracy. Therefore, it is completely justifiable to consider the current S-DSM as an exact method. In addition, it should be emphasised that unlike the other existing methods, the present method is a much more versatile method providing a unified S-DS matrix to deal with arbitrarily prescribed boundary conditions.

## 7. Conclusions

An exact spectral dynamic stiffness method (S-DSM) has been developed for free vibration analysis of rectangular plates with arbitrary boundary conditions. This has been achieved based on a general solution satisfying the governing differential equation exactly. The S-DSM has been formulated in a systematic way making use of symbolic calculation. The method provides a unified solution to obtain the natural frequencies for any arbitrary boundary conditions. By means of the modified Fourier series, any prescribed boundary conditions can be transformed into displacement or force vectors which are related by the spectral-dynamic stiffness matrix. The modified Fourier series was introduced to keep the symplecticity of the formulation, so as to facilitate the application of the Wittrick–Williams algorithm. As the solution technique, the Wittrick–Williams algorithm has been enhanced with several elegant and efficient techniques. The S-DSM solutions have been validated by and compared with a wide range of existing exact

and analytical solutions. The computed S-DSM results are accurate to all figures presented, which can serve as benchmark solutions. The superiority of the proposed S-DSM has been demonstrated in terms of its excellent computational efficiency, accuracy and robustness. It has been shown that the proposed S-DSM has as much as 100-fold advantage in computational speed over the conventional finite element method. Based on the comparison, a comprehensive discussion has been made for a wide range of analytical methods for free vibration analysis of plates where significant physical and mathematical insights have been gained. Some instructive conclusions have been drawn for general series-based analytical (and exact) solutions. The proposed method has recently been extended by the authors to complex composite plate assemblies [74,75] with non-classical boundary conditions which include uniform or non-uniform elastic constraints [76], point or partial supports or a mixture of them in any combination.

## Acknowledgements

The authors appreciate the support given by EPSRC, UK through a Grant EP/J007706/1 which made this work possible. The authors are also grateful to Prof. Stanislav Papkov (Sevastopol National Technical University) for many stimulating discussions.

## Appendix A. Modified Fourier basis function and the corresponding modified Fourier series

The general solution of the GDE with unspecified boundary conditions is pursued by using the spectral method [77]. Any arbitrary one-dimensional function $f(\xi), \xi \in [-L, L]$ can be represented by the following modified Fourier basis function.

$$\mathcal{T}_l(\gamma_{ls}\xi) = \begin{cases} \cos\left(\frac{s\pi}{L}\xi\right) & l = 0 \\ \sin\left(\left(s+\frac{1}{2}\right)\frac{\pi}{L}\xi\right) & l = 1 \end{cases}, \quad \xi \in [-L, L], \quad s \in \mathbb{N}, \tag{A.1}$$

where $\mathbb{N} = \{0, 1, 2, \ldots\}$ is the non-negative integers set. It can be proved mathematically that the above basis functions form a complete orthogonal set.

As pointed out by Bracewell [78], there are three versions of Fourier series transformation formula in common use, in which the third version provides the symmetry of the forward and inverse Fourier transformation, and importantly, it can eliminate the dependence of the length of the integral range. Therefore, $f(\xi)$ can represented by the modified Fourier series as follows

$$f(\xi) = \sum_{\substack{s\in\mathbb{N} \\ l\in\{0,1\}}} F_{ls}\frac{\mathcal{T}_l(\gamma_{ls}\xi)}{\sqrt{\zeta_{ls}L}}, \quad F_{ls} = \int_{-L}^{L} f(\xi)\frac{\mathcal{T}_l(\gamma_{ls}\xi)}{\sqrt{\zeta_{ls}L}}\mathrm{d}\xi, \tag{A.2}$$

where $s \in \mathbb{N}$ and

$$\zeta_{ls} = \begin{cases} 2 & l = 0 \text{ and } s = 0 \\ 1 & l = 1 \text{ or } s \geqslant 1 \end{cases}. \tag{A.3}$$

The hyperbolic functions $\mathcal{H}_l(\Gamma\xi)$ with the definitions in Eq. (13) can be transformed into Fourier series as follows based on Eq. (A.2):

$$\mathcal{H}_l(\Gamma\xi) = \sum_{s\in\mathbb{N}} \frac{2(-1)^s \Gamma\mathcal{H}_l^*(\Gamma L)}{\sqrt{\zeta_{ls}L}(\Gamma^2+\gamma_{ls}^2)}\frac{\mathcal{T}_l(\gamma_{ls}\xi)}{\sqrt{\zeta_{ls}L}}, \tag{A.4}$$

where $\mathcal{H}_l^*(\Gamma L) = \mathrm{d}\mathcal{H}_l(\Gamma\xi)/(\Gamma\mathrm{d}\xi)|_{\xi=L}$ following the definition of Eq. (15).

## Appendix B. Infinite sets of algebraic equations based on Eq. (20)

The expressions of $W_a^{kj}$ and $W_b^{kj}$ in Eq. (20a) yield the following two equations respectively

$$\begin{aligned} W^{kj}\big|_{x=a} &= \sum_{m\in\mathbb{N}}(-1)^m\left[A_{1km}\mathcal{H}_j(p_{1km}y) + A_{2km}\mathcal{H}_j(p_{2km}y)\right] \\ &\quad + \sum_{n\in\mathbb{N}}\left[B_{1jn}\mathcal{H}_k(q_{1jn}a) + B_{2jn}\mathcal{H}_k(q_{2jn}a)\right]\mathcal{T}_j(\beta_{jn}y) \\ &= \sum_{n\in\mathbb{N}} W_{ajn}\mathcal{T}_j(\beta_{jn}y)/\sqrt{\zeta_{jn}b}, \end{aligned} \tag{B.1a}$$

$$\begin{aligned} W^{kj}\big|_{y=b} &= \sum_{n\in\mathbb{N}}(-1)^n\left[B_{1jn}\mathcal{H}_k(q_{1jn}x) + B_{2jn}\mathcal{H}_k(q_{2jn}x)\right] \\ &\quad + \sum_{m\in\mathbb{N}}\left[A_{1km}\mathcal{H}_j(p_{1km}b) + A_{2km}\mathcal{H}_j(p_{2km}b)\right]\mathcal{T}_k(\alpha_{km}x) \\ &= \sum_{m\in\mathbb{N}} W_{bkm}\mathcal{T}_k(\alpha_{km}x)/\sqrt{\zeta_{km}a}, \end{aligned} \tag{B.1b}$$

The two infinite sets of algebraic equation can be obtained by first substituting the expressions for $A_{1km}, A_{2km}, B_{1jn}$ and $B_{2jn}$ in Eqs. (24) and (25) into $W_a^{kj}$ and $W_a^{kj}$ in Eq. (20) and then applying the Fourier series formulae of Eq. (A.4) on the hyperbolic functions to give

$$\begin{aligned} W_{ajn} &= \sum_{m\in\mathbb{N}} \frac{2(-1)^{m+n}\left[V_{bkm} - \left(\nu\alpha_{km}^2 + \beta_{jn}^2\right)\phi_{bkm}/\zeta_{km}\right]}{\sqrt{ab}(p_{1km}^2+\beta_{jn}^2)(p_{2km}^2+\beta_{jn}^2)} \\ &\quad + \frac{1}{\sqrt{\chi^2+4\kappa}}\left\{\left[\zeta_{jn}V_{ajn} - \left(\nu\beta_{jn}^2 - q_{1jn}^2\right)\phi_{ajn}\right]\frac{\mathcal{TH}_k(q_{1jn}a)}{q_{1jn}}\right. \\ &\quad \left. - \left[\zeta_{jn}V_{ajn} - \left(\nu\beta_{jn}^2 - q_{2jn}^2\right)\phi_{ajn}\right]\frac{\mathcal{TH}_k(q_{2jn}a)}{q_{2jn}}\right\} \end{aligned} \tag{B.2}$$

and

$$\begin{aligned} W_{bkm} &= \frac{1}{\sqrt{\chi^2+4\kappa}}\left\{\left[\zeta_{km}V_{bkm} - \left(\nu\alpha_{km}^2 - p_{1km}^2\right)\phi_{bkm}\right]\frac{\mathcal{TH}_j(p_{1km}b)}{p_{1km}}\right. \\ &\quad \left. - \left[\zeta_{km}V_{bkm} - \left(\nu\alpha_{km}^2 - p_{2km}^2\right)\phi_{bkm}\right]\frac{\mathcal{TH}_j(p_{2km}b)}{p_{2km}}\right\} \\ &\quad + \sum_{n\in\mathbb{N}} \frac{2(-1)^{m+n}\left[V_{ajn} - \left(\alpha_{km}^2 + \nu\beta_{jn}^2\right)\phi_{ajn}/\zeta_{jn}\right]}{\sqrt{ab}(q_{1jn}^2+\alpha_{km}^2)(q_{2jn}^2+\alpha_{km}^2)}, \end{aligned} \tag{B.3}$$

where $\mathcal{TH}_l(\Xi) = \mathcal{H}_l(\Xi)/\mathcal{H}_l^*(\Xi)$. Another two infinite sets of algebraic equations based on $M_a^{kj}$ and $M_b^{kj}$ can be arrived at following analogous procedure as above. Finally these four infinite sets of equations can be rewritten in matrix form as shown in Eq. (26).

## Appendix C. Analytical expressions for the coefficient matrices in Eq. (26)

The notations introduced earlier make the expressions for the coefficient matrices of Eq. (26) highly symbolic and simplified and thus easy to be implemented in a computer program.

If the numbers of terms in the series in $x$ and $y$ coordinates are $M$ and $N$ respectively (i.e., $m \in [0, M-1]$ and $n \in [0, N-1]$), all of the four matrices $\boldsymbol{A}_{W\Phi}^{kj}, \boldsymbol{A}_{WV}^{kj}, \boldsymbol{A}_{M\Phi}^{kj}$ and $\boldsymbol{A}_{MV}^{kj}$ will be $(M+N)\times(M+N)$ matrices with the same structure as follows:

$$\boldsymbol{A} = \left[\begin{array}{ccc:ccc} \boldsymbol{A}(n,n)|_{n=0} & & 0 & \boldsymbol{A}(n,m)|_{\substack{n=0\\m=0}} & \cdots & \boldsymbol{A}(n,m)|_{\substack{n=0\\m=M-1}} \\ & & & & & \\ 0 & \ddots & 0 & \vdots & \ddots & \vdots \\ 0 & 0 & \boldsymbol{A}(n,n)|_{n=N-1} & \boldsymbol{A}(n,m)|_{\substack{n=N-1\\m=0}} & \cdots & \boldsymbol{A}(n,m)|_{\substack{n=N-1\\m=M-1}} \\ \hdashline \boldsymbol{A}(m,n)|_{\substack{m=0\\n=0}} & \cdots & \boldsymbol{A}(m,n)|_{\substack{m=0\\n=N-1}} & \boldsymbol{A}(m,m)|_{m=0} & 0 & 0 \\ & & & & & \\ \vdots & \ddots & \vdots & 0 & \ddots & 0 \\ \boldsymbol{A}(m,n)|_{\substack{m=M-1\\n=0}} & \cdots & \boldsymbol{A}(m,n)|_{\substack{m=M-1\\n=N-1}} & 0 & 0 & \boldsymbol{A}(m,m)|_{m=M-1} \end{array}\right] \tag{C.1}$$

The entries of these four matrices can be expressed in a concise and simplified form as

$$\boldsymbol{A}^{kj}_{W\Phi}(n,n) = -(\Sigma_1\Upsilon_1 - \Sigma_2\Upsilon_2)/\Upsilon_0 \quad \boldsymbol{A}^{kj}_{W\Phi}(n,m) = -\Sigma_5\Sigma_7$$
$$\boldsymbol{A}^{kj}_{W\Phi}(m,n) = -\Sigma_6\Sigma_8 \quad \boldsymbol{A}^{kj}_{W\Phi}(m,m) = -(\Sigma_3\Upsilon_3 - \Sigma_4\Upsilon_4)/\Upsilon_0$$
$$\boldsymbol{A}^{kj}_{WV}(n,n) = (\Upsilon_1 - \Upsilon_2)/\Upsilon_0 \quad \boldsymbol{A}^{kj}_{WV}(n,m) = \Sigma_7$$
$$\boldsymbol{A}^{kj}_{WV}(m,n) = \Sigma_8 \quad \boldsymbol{A}^{kj}_{WV}(m,m) = (\Upsilon_3 - \Upsilon_4)/\Upsilon_0$$
$$\boldsymbol{A}^{kj}_{M\Phi}(n,n) = -(\Sigma_1^2\Upsilon_1 - \Sigma_2^2\Upsilon_2)/\Upsilon_0 \quad \boldsymbol{A}^{kj}_{M\Phi}(n,m) = -\Sigma_9\Sigma_7$$
$$\boldsymbol{A}^{kj}_{M\Phi}(m,n) = -\Sigma_9\Sigma_8 \quad \boldsymbol{A}^{kj}_{M\Phi}(m,m) = -(\Sigma_3^2\Upsilon_3 - \Sigma_4^2\Upsilon_4)/\Upsilon_0$$
$$\boldsymbol{A}^{kj}_{MV}(n,n) = (\Sigma_1\Upsilon_1 - \Sigma_2\Upsilon_2)/\Upsilon_0 \quad \boldsymbol{A}^{kj}_{MV}(n,m) = \Sigma_6\Sigma_7$$
$$\boldsymbol{A}^{kj}_{MV}(m,n) = \Sigma_5\Sigma_8 \quad \boldsymbol{A}^{kj}_{MV}(m,m) = (\Sigma_3\Upsilon_3 - \Sigma_4\Upsilon_4)/\Upsilon_0$$

where

$$\Upsilon_0 = \sqrt{\chi^2 + 4\kappa}, \qquad \Sigma_0 = 2(-1)^{m+n},$$
$$\Upsilon_1 = \mathcal{TH}_k(q_{1jn}a)/q_{1jn}, \quad \Upsilon_2 = \mathcal{TH}_k(q_{2jn}a)/q_{2jn},$$
$$\Upsilon_3 = \mathcal{TH}_j(p_{1km}b)/p_{1km}, \quad \Upsilon_4 = \mathcal{TH}_j(p_{2km}b)/p_{2km},$$
$$\Sigma_1 = \nu\beta_{jn}^2 - q_{1jn}^2, \qquad \Sigma_2 = \nu\beta_{jn}^2 - q_{2jn}^2,$$
$$\Sigma_3 = \nu\alpha_{km}^2 - p_{1km}^2, \qquad \Sigma_4 = \nu\alpha_{km}^2 - p_{2km}^2,$$
$$\Sigma_5 = \nu\alpha_{km}^2 + \beta_{jn}^2, \qquad \Sigma_6 = \alpha_{km}^2 + \nu\beta_{jn}^2,$$
$$\Sigma_7 = \Sigma_0 \Big/ \left[\sqrt{\zeta_{jn}\zeta_{km}ab}(p_{1km}^2 + \beta_{jn}^2)(p_{2km}^2 + \beta_{jn}^2)\right],$$
$$\Sigma_8 = \Sigma_0 / \left[\sqrt{\zeta_{jn}\zeta_{km}ab}(q_{1jn}^2 + \alpha_{km}^2)(q_{2jn}^2 + \alpha_{km}^2)\right],$$
$$\Sigma_9 = (1-\nu)^2\alpha_{km}^2\beta_{jn}^2 + \nu\kappa + \nu(\alpha_{km}^2 + \beta_{jn}^2)\chi,$$

where $\mathcal{TH}_l(\Xi) = \mathcal{H}_l(\Xi)/\mathcal{H}_l^*(\Xi)$. It should be highlighted that the above expressions are applicable for the four symmetric/antisymmetric component cases with the superscripts $kj$ taking the values '00','01','10' and '11', respectively. Moreover, the above analytical expressions have clear physical meanings. For example, $\chi$ is the rotatory inertia parameter which takes zero when the rotatory inertia is not taken into account. Also, $\alpha_{km}, \beta_{jn}$ are wavenumbers and $p_{1km}, p_{2km}, q_{1jn}, q_{2jn}$ are frequency-dependent wave parameters. It is clear that $\Sigma_7 = \Sigma_8$ based on Eq. (18d). Therefore, $\boldsymbol{A}^{kj}_{WV}$ and $\boldsymbol{A}^{kj}_{M\Phi}$ are symmetric matrices, and $\boldsymbol{A}^{kj}_{W\Phi} = -\boldsymbol{A}^{kj\,T}_{MV}$. This is owing to the reciprocal principle and the Fourier series formula (A.2) adopted in the formulation. In addition, the two sub-matrices for each symmetry component case in the diagonal position corresponding to $\boldsymbol{A}(n,n)$ and $\boldsymbol{A}(m,m)$ are diagonal matrices. This is due to the fact that all of the frequency-wavenumber dependent DOFs in one direction (for the corresponding displacement or force) are strictly orthogonal to each other. The strict orthogonality of the formulation enable the evaluation at any high values of $M$ and $N$, which guarantees the unconditionally numerical stability of the current method.

## Appendix D. Supplementary material

Supplementary data associated with this article can be found, in the online version, at http://dx.doi.org/10.1016/j.compstruc.2015.11.005.

## References


[1] Chladni EFF, Die Akustik, Breitkopf und Hartel, Leipzig; 1802.
[2] Rayleigh Lord. The theory of sound, vol. I. London: Macmilllan and Co.; 1877.
[3] Ritz W. Theorie der Transversalschwingungen einer quadratischen Platte mit freien Rändern. Ann Phys 1909;333(4):737–86. http://dx.doi.org/10.1002/andp.19093330403.
[4] Lévy M. Sur l'équilibre élastique d'une plaque rectangulaire. Comptea Rendus 1899;129:535–9.
[5] Bert CW, Malik M. Frequency equations and modes of free vibrations of rectangular plates with various edge conditions. Proc Inst Mech Eng Part C: J Mech Eng Sci 1994;208:307–19. http://dx.doi.org/10.1243/PIME_PROC_1994_208_133_02.
[6] Kantorovich LV, Krylov VI. Approximate methods of higher analysis. Groningen: Noordhoff; 1958.
[7] Gorman DJ. Vibration analysis of plates by the superposition method. London: World Scientific; 1999.
[8] Gorman DJ, Yu SD. A review of the superposition method for computing free vibration eigenvalues of elastic structures. Comput Struct 2012;104–105:27–37. http://dx.doi.org/10.1016/j.compstruc.2012.02.018.
[9] Kshirsagar S, Bhaskar K. Accurate and elegant free vibration and buckling studies of orthotropic rectangular plates using untruncated infinite series. J Sound Vib 2008;314(3-5):837–50. http://dx.doi.org/10.1016/j.jsv.2008.01.013.
[10] Meleshko VV, Papkov SO. Flexural vibrations of elastic rectangular plate with free edges - from Frigid (1809) and the Ritz (1909) up to now. Acoust Bull 2009;12(4):34–51 [in Russian].
[11] Li WL, Zhang X, Du J, Liu Z. An exact series solution for the transverse vibration of rectangular plates with general elastic boundary supports. J Sound Vib 2009;321(1–2):254–69. http://dx.doi.org/10.1016/j.jsv.2008.09.035.
[12] Khov H, Li WL, Gibson RF. An accurate solution method for the static and dynamic deflections of orthotropic plates with general boundary conditions. Compos Struct 2009;90(4):474–81. http://dx.doi.org/10.1016/j.compstruct.2009.04.020.
[13] Leung AYT. Dynamic stiffness and substructures. London: Springer London; 1993. http://dx.doi.org/10.1007/978-1-4471-2026-1.
[14] Warburton GB. The vibration of rectangular plates. Proc Inst Mech Eng 1954;168(1):371–84. http://dx.doi.org/10.1243/PIME_PROC_1954_168_040_02.
[15] Leissa AW. The free vibration of rectangular plates. J Sound Vib 1973;31(3):257–93. http://dx.doi.org/10.1016/S0022-460X(73)80371-2.
[16] Bhat RB. Natural frequencies of rectangular plates using characteristic orthogonal polynomials in Rayleigh–Ritz method. J Sound Vib 1985;102(4):493–9. http://dx.doi.org/10.1016/S0022-460X(85)80109-7.
[17] Dickinson SM, Blasio AD. On the use of orthogonal polynomials in the Rayleigh–Ritz method for the study of the flexural vibration and buckling of isotropic and orthotropic rectangular plates. J Sound Vib 1986;108(1):51–62. http://dx.doi.org/10.1016/S0022-460X(86)80310-8.
[18] Kim CS, Young PG, Dickinson SM. On the flexural vibration of rectangular plates approached by using simple polynomials in the Rayleigh–Ritz method. J Sound Vib 1990;143(3):379–94. http://dx.doi.org/10.1016/0022-460X(90)90730-N.
[19] Liew KM, Lam KY, Chow ST. Free vibration analysis of rectangular plates using orthogonal plate functions. Comput Struct 1990;34(1):79–85. http://dx.doi.org/10.1016/0045-7949(90)90302-I.
[20] Liew KM, Wang CM. Vibration analysis of plates by the pb-2 Rayleigh–Ritz method: mixed boundary conditions, reentrant corners, and internal curved supports. Mech Struct Mach 1992;20(3):281–92. http://dx.doi.org/10.1080/08905459208905170.
[21] Liew KM, Wang CM. pb-2 Rayleigh–Ritz method for general plate analysis. Eng Struct 1993;15(1):55–60. http://dx.doi.org/10.1016/0141-0296(93)90017-X.
[22] Lim CW, Liew KM. A pb-2 Ritz formulation for flexural vibration of shallow cylindrical shells of rectangular planform. J Sound Vib 1994;173(3):343–75. http://dx.doi.org/10.1006/jsvi.1994.1235.
[23] Beslin O, Nicolas J. A hierarchical functions set for predicting very high order plate bending modes with any boundary conditions. J Sound Vib 1997;202(5):633–55. http://dx.doi.org/10.1006/jsvi.1996.0797.
[24] Dozio L. On the use of the Trigonometric Ritz method for general vibration analysis of rectangular Kirchhoff plates. Thin-Walled Struct 2011;49(1):129–44. http://dx.doi.org/10.1016/j.tws.2010.08.014.
[25] Zhou D. Natural frequencies of elastically restrained rectangular plates using a set of static beam functions in the Rayleigh–Ritz method. Comput Struct 1995;57(4):731–5. http://dx.doi.org/10.1016/0045-7949(95)00066-P.
[26] Cheung YK, Zhou D. Vibrations of rectangular plates with elastic intermediate line-supports and edge constraints. Thin-Walled Struct 2000;37:305–31. http://dx.doi.org/10.1016/S0263-8231(00)00015-X.
[27] Zhou D. Vibrations of point-supported rectangular plates with variable thickness using a set of static tapered beam functions. Int J Mech Sci 2002;44:149–64. http://dx.doi.org/10.1016/S0020-7403(01)00081-9.
[28] Li WL. Vibration analysis of rectangular plates with general elastic boundary supports. J Sound Vib 2004;273(3):619–35. http://dx.doi.org/10.1016/S0022-460X(03)00562-5.
[29] Monterrubio LE, Ilanko S. Proof of convergence for a set of admissible functions for the Rayleigh–Ritz analysis of beams and plates and shells of rectangular planform. Comput Struct 2015;147:236–43. http://dx.doi.org/10.1016/j.compstruc.2014.09.008.
[30] Kerr AD. An extended Kantorovich method for the solution of eigenvalue problems. Int J Solids Struct 1969;5:559–72. http://dx.doi.org/10.1016/0020-7683(69)90028-6.
[31] Jones R, Milne BJ. Application of the extended Kantorovich method to the vibration of clamped rectangular plates. J Sound Vib 1976;45(3):309–16. http://dx.doi.org/10.1016/0022-460X(76)90390-4.
[32] Sakata T, Takahashi K, Bhat RB. Natural frequencies of orthotropic rectangular plates obtained by iterative reduction of the partial differential equation. J Sound Vib 1996;189(1):89–101. http://dx.doi.org/10.1006/jsvi.1996.9999.

[33] Rajalingham C, Bhat RB, Xistris GD. Vibration of rectangular plates by reduction of the plate partial differential equation into simultaneous ordinary differential equations. J Sound Vib 1997;203(1):169–80. http://dx.doi.org/10.1006/jsvi.1996.0814.
[34] Lamé MG. Leçons sur la théorie mathématique: de l'élasticité des corps solides. Bachelier, Paris; 1852.
[35] Iguchi S. Die Eigenschwingungen und Klangfiguren der vierseitig freien rechteckigen Platte. Mem Faculty Eng Hokkaido Imperial Univ 1942;6 (5):317–85. http://dx.doi.org/10.1007/BF00535853.
[36] Papkov SO, Banerjee JR. A new method for free vibration and buckling analysis of rectangular orthotropic plates. J Sound Vib 2015;339:342–58. http://dx.doi.org/10.1016/j.jsv.2014.11.007.
[37] Papkov SO. The generalization of Koialovich's asymptotic law on a case of the nongegative infinite matrix. Dinamicheskie Sistemy (Simferopol') 2011;1 (29):255–67 [in Russian].
[38] Sakata T, Hosokawa K. Vibrations of clamped orthotropic rectangular plates. J Sound Vib 1988;125(3):429–39. http://dx.doi.org/10.1016/0022-460X(88)90252-0.
[39] Xing YF, Liu B. New exact solutions for free vibrations of rectangular thin plates by symplectic dual method. Acta Mech Sin 2008;25(2):265–70. http://dx.doi.org/10.1007/s10409-008-0208-4.
[40] Xing YF, Liu B. New exact solutions for free vibrations of thin orthotropic rectangular plates. Compos Struct 2009;89(4):567–74. http://dx.doi.org/10.1016/j.compstruct.2008.11.010.
[41] Xing YF, Xu TF. Solution methods of exact solutions for free vibration of rectangular orthotropic thin plates with classical boundary conditions. Compos Struct 2013;104:187–95. http://dx.doi.org/10.1016/j.compstruct.2013.04.030.
[42] Bahrami A, Bahrami MN, Ilkhani MR. Comments on New exact solutions for free vibrations of thin orthotropic rectangular plates. Compos Struct 2014;107:745–6. http://dx.doi.org/10.1016/j.compstruct.2013.09.064.
[43] Lim CW, Xu XS. Symplectic elasticity: theory and applications. Appl Mech Rev 2010;63:050802. http://dx.doi.org/10.1115/1.4003700.
[44] Lim CW, Lü CF, Xiang Y, Yao W. On new symplectic elasticity approach for exact free vibration solutions of rectangular Kirchhoff plates. Int J Eng Sci 2009;47:131–40. http://dx.doi.org/10.1016/j.ijengsci.2008.08.003.
[45] Lim CW. Symplectic elasticity approach for free vibration of rectangular plates. Adv Vib Eng 2010;9(2):159–63.
[46] Lee U. Spectral element method in structural dynamics. Singapore: John Wiley & Sons; 2009.
[47] Wittrick WH, Williams FW. A general algorithm for computing natural frequencies of elastic structures. Q J Mech Appl Math XXIV 1971(3):263–84. http://dx.doi.org/10.1093/qjmam/24.3.263.
[48] Wittrick WH, Williams FW. Buckling and vibration of anisotropic or isotropic plate assemblies under combined loadings. Int J Mech Sci 1974;16(4):209–39. http://dx.doi.org/10.1016/0020-7403(74)90069-1.
[49] Boscolo M, Banerjee JR. Dynamic stiffness elements and their applications for plates using first order shear deformation theory. Comput Struct 2011;89(3-4):395–410. http://dx.doi.org/10.1016/j.compstruc.2010.11.005.
[50] Boscolo M, Banerjee JR. Dynamic stiffness formulation for composite Mindlin plates for exact modal analysis of structures. Part I: theory. Comput Struct 2012;96-97:61–73. http://dx.doi.org/10.1016/j.compstruc.2012.01.002.
[51] Boscolo M, Banerjee JR. Dynamic stiffness formulation for composite Mindlin plates for exact modal analysis of structures. Part II: results and applications. Comput Struct 2012;96–97:74–83. http://dx.doi.org/10.1016/j.compstruc.2012.01.003.
[52] Fazzolari FA, Boscolo M, Banerjee JR. An exact dynamic stiffness element using a higher order shear deformation theory for free vibration analysis of composite plate assemblies. Compos Struct 2013;96:262–78. http://dx.doi.org/10.1016/j.compstruct.2012.08.033.
[53] Boscolo M, Banerjee JR. Layer-wise dynamic stiffness solution for free vibration analysis of laminated composite plates. J Sound Vib 2014;333 (1):200–27. http://dx.doi.org/10.1016/j.jsv.2013.08.031.
[54] Patera AT. A spectral element method for fluid dynamics: laminar flow in a channel expansion. J Comput Phys 1984;54:468–88. http://dx.doi.org/10.1016/0021-9991(84)90128-1.
[55] Ostachowicz W, Kudela P, Krawczuk M, Zak A. Guided waves in structures for SHM: the time – domain spectral element method. New Delhi: Wiley; 2012.
[56] Reddy JN. Mechanics of laminated composite plates and shells theory and analysis. 2nd ed. CRC Press; 2003.
[57] Zhong WX. Duality system in applied mechanics and optimal control. London: Kluwer Academic Publishers; 2004.
[58] Howson WP, Williams FW. Natural frequencies of frames with axially loaded Timoshenko Members. J Sound Vib 1973;26(4):503–15. http://dx.doi.org/10.1016/S0022-460X(73)80216-0.
[59] Banerjee JR, Williams FW. Clamped-clamped natural frequencies of a bending-torsion coupled beam. J Sound Vib 1994;176(3):301–6. http://dx.doi.org/10.1006/jsvi.1994.1378.
[60] Hardy GH. Ramanujan: twelve lectures on subjects suggested by his life and work. 3rd ed. New York: AMS Chelsea Publishing; 1999.
[61] Filipich CP, Rosales MB. Arbitrary precision frequencies of a free rectangular thin plate. J Sound Vib 2000;230(3):521–39. http://dx.doi.org/10.1006/jsvi.1999.2629.
[62] Mochida Y. The boundedness of Gormans Superposition method for free vibration analysis of plates. Comput Struct 2012;104-105:38–43. http://dx.doi.org/10.1016/j.compstruc.2012.03.009.
[63] Malik M, Bert CW. Three-dimensional elasticity solutions for free vibrations of rectangular plates by the differential quadrature method. Int J Solids Struct 1998;35(3–4):299–318. http://dx.doi.org/10.1016/S0020-7683(97)00073-5.
[64] Leissa AW, Narita Y. Vibrations of completely free shallow shells of rectangular planform. J Sound Vib 1984;96(2):207–18. http://dx.doi.org/10.1016/0022-460X(84)90579-0.
[65] Gorman DJ. Free vibration analysis of the completely free rectangular plate by the method of superposition. J Sound Vib 1978;57(3):437–47. http://dx.doi.org/10.1006/jsvi.2000.3151.
[66] Rosales MB, Filipich CP. Vibration of orthotropic plates: discussion on the completeness of the solutions used in direct methods. J Sound Vib 2003;261 (4):751–7. http://dx.doi.org/10.1016/S0022-460X(02)01174-4.
[67] Ng CHW, Zhao YB, Wei GW. Comparison of discrete singular convolution and generalized differential quadrature for the vibration analysis of rectangular plates. Comput Methods Appl Mech Eng 2004;193(23-26):2483–506. http://dx.doi.org/10.1016/j.cma.2004.01.013.
[68] Rajalingham C, Bhat RB, Xistris GD. Vibration of rectangular plates using plate characteristic functions as shape functions in the Rayleigh–Ritz method. J Sound Vib 1996;193(2):497–509. http://dx.doi.org/10.1006/jsvi.1996.0298.
[69] Leissa AW. Vibration of plates. Tech. rep., Ohio State University, Ohio; 1969.
[70] Gorman DJ. Free vibration analysis of cantilever plates by the method of superposition. J Sound Vib 1976;49(4):453–67. http://dx.doi.org/10.1016/0022-460X(76)90828-2.
[71] Courant R, Hilbert D. Methods of mathematical physics, vol. I. Heidelberg: Interscience; 1953.
[72] Zhou D. Natural frequencies of rectangular plates using a set of static beam functions in Rayleigh–Ritz method. J Sound Vib 1996;189:81–7. http://dx.doi.org/10.1006/jsvi.1996.0006.
[73] Hurlebaus S, Gaul L, Wang JTS. An exact series solution for calculating the eigenfrequencies of orthotropic plates with completely free boundary. J Sound Vib 2001;244(5):747–59. http://dx.doi.org/10.1006/jsvi.2000.3541.
[74] Liu X, Banerjee JR. An exact spectral-dynamic stiffness method for free flexural vibration analysis of orthotropic composite plate assemblies – part I: theory. Compos Struct 2015;132:1274–87. http://dx.doi.org/10.1016/j.compstruct.2015.07.020.
[75] Liu X, Banerjee JR. An exact spectral-dynamic stiffness method for free flexural vibration analysis of orthotropic composite plate assemblies – part II: applications. Compos Struct 2015(132):1288–302. http://dx.doi.org/10.1016/j.compstruct.2015.07.022.
[76] Liu X, Kassem HI, Banerjee JR. Spectral-dynamic stiffness theory for modal analysis of composite plate-like structures with arbitrary non-uniform elastic supports, coupling constraints and mass attachments. Compos Struct [submitted for publication].
[77] Boyd JP. Chebyshev and fourier spectral methods. 2nd ed. New: Dover Publications; 2001.
[78] Bracewell RN. The fourier transform and its applications. 2nd ed. London: McGraw-Hill Book Company; 1978.